Accurate multilayered shell buckling analysis via the implicit-mesh discontinuous Galerkin method *

Giuliano Guarino†
Department of Engineering, Università degli Studi di Palermo, 90128, Italy

Vincenzo Gulizzi‡
Department of Engineering, Università degli Studi di Palermo, 90128, Italy
Lawrence Berkeley National Laboratory MS 50A-3111, Berkeley, CA 94720, USA

Alberto Milazzo§
Department of Engineering, Università degli Studi di Palermo, 90128, Italy

A novel formulation for the linear buckling analysis of multilayered shells is presented. High-order equivalent-single-layer shell theories based on the through-the-thickness expansion of the covariant components of the displacement field are employed. The novelty of the formulation regards the governing equations solution via implicit-mesh discontinuous Galerkin method. It is a high-order accurate numerical technique based on a discontinuous representation of the solution among the mesh elements and on the use of suitably defined boundary integrals to enforce the continuity of the solution at the inter-element interfaces as well as the boundary conditions. Owing to its discontinuous nature, it can be naturally employed with non-conventional meshes. In this work, it is combined with the implicitly-defined mesh technique, whereby the mesh of the shell modelling domain is constructed by intersecting an easy-to-generate background grid and a level set function implicitly representing the cutouts. Several numerical examples are considered for the buckling loads of plates and cylinders modelled by different shell theories and characterized by various materials, geometry, boundary conditions and cutouts. The obtained results are compared with literature and finite-element solutions and they demonstrate the accuracy and the robustness of the proposed approach.

I. Nomenclature

$V, \partial V$	=	shell volume and boundary
τ	=	shell thickness
N_ℓ	=	shell number of layers
$V^{\langle\ell\rangle}, \partial V^{\langle\ell\rangle}$	=	ℓ-th layer volume and boundary
$\tau^{\langle\ell\rangle}$	=	ℓ-th layer thickness
$\theta^{\langle\ell\rangle}$	=	ℓ-th layer lamination angle
(ξ_1, ξ_2, ξ_3)	=	curvilinear coordinates
$\Omega_\xi, \partial\Omega_\xi$	=	shell modelling domain and boundary
$I_{\xi_3}, I_{\xi_3}^{\langle\ell\rangle}$	=	thickness interval for the shell and for the ℓ-th layer
$\xi_{3b}^{\langle\ell\rangle}, \xi_{3t}^{\langle\ell\rangle}$	=	values of ξ_3 identifying the bottom and top surfaces of the ℓ-th layer
$\boldsymbol{x}_0, \boldsymbol{x}$	=	point on the shell mean surface and in the shell volume
$\boldsymbol{n}_0$	=	unit vector orthogonal to the shell mean surface
$\boldsymbol{g}_i$	=	i-th vector of the covariant basis
$\boldsymbol{g}^i$	=	i-th vector of the contravariant basis
$\boldsymbol{R}_\xi$	=	transformation matrix
g_{ij}	=	ij-th covariant component of the metric tensor
g^{ij}	=	ij-th contravariant component of the metric tensor
g	=	determinant of g_{ij}
$\boldsymbol{u}$	=	vector of the displacement Cartesian components
$\boldsymbol{u}_\xi$	=	vector of the displacement covariant components
$\boldsymbol{Z}$	=	matrix of the thickness functions
$\boldsymbol{U}$	=	vector of the generalized displacements

* The present work was presented at the AIAA Science and Technology Forum that was held in San Diego from the 3rd to the 7th of January 2022 with the ID AIAA-2022-1490.

†Ph.D. Student, Dipartimento di Ingegneria, Viale delle Scienze, Building 8. Student Member AIAA.
‡Assistant Professor, Dipartimento di Ingegneria, Viale delle Scienze, Building 8, Regular Member AIAA.
§Professor, Dipartimento di Ingegneria, Viale delle Scienze, Building 8; alberto.milazzo@unipa.it. Senior Member AIAA.

$\boldsymbol{\gamma}$	=	vector of the strain Cartesian components (Voigt notation)
$\boldsymbol{D}_{0i}, \boldsymbol{D}_{\alpha i}$	=	auxiliary matrices linking the derivatives of the displacement vector with the generalized displacements
$\boldsymbol{J}_0, \boldsymbol{J}_\alpha$	=	auxiliary matrices linking the strain vector with the generalized displacements
$\boldsymbol{m}_i^{\langle\ell\rangle}$	=	i-th vector of the orthotropy reference system for the ℓ-th layer
$\widetilde{\boldsymbol{\sigma}}^{\langle\ell\rangle}$	=	vector of the stress Cartesian components in the orthotropy reference system (Voigt notation)
$\boldsymbol{\sigma}^{\langle\ell\rangle}$	=	vector of the stress Cartesian components in the global reference system (Voigt notation)
$\widetilde{\boldsymbol{c}}^{\langle\ell\rangle}, \boldsymbol{c}^{\langle\ell\rangle}$	=	stiffness matrix in the orthotropy and in the global reference systems
$\overline{\boldsymbol{b}}, \overline{\boldsymbol{t}}$	=	prescribed volume force and boundary traction fields
$\boldsymbol{Q}_{\alpha\beta}, \boldsymbol{R}_{\alpha 3}, \boldsymbol{S}_{33}$	=	generalized stiffness matrices
$\overline{\boldsymbol{B}}, \overline{\boldsymbol{T}}$	=	prescribed generalized volume and boundary loads
$\overline{\boldsymbol{U}}$	=	prescribed generalized displacements
$\overline{\sigma}_{ij}$	=	ij-th component of the initial stress field
λ	=	buckling eigenvalue
$\boldsymbol{Q}^G_{\alpha\beta}, \boldsymbol{R}^G_{\alpha 3}, \boldsymbol{S}^G_{33}$	=	generalized geometric stiffness matrices
N_e	=	number of mesh elements
Ω^e_ξ	=	e-the mesh element
$\partial\Omega^e_{\xi D}, \partial\Omega^e_{\xi N}$	=	boundary of the e-th element where Dirichlet and Neumann boundary conditions are enforced
Ω^h_ξ	=	approximated modelling domain
$\mathcal{V}^N_{hp}$	=	space of N-dimensional discontinuous vector fields
$\mathcal{P}^e_p$	=	space of polynomial functions of degree at most p over the e-th element
$\partial\Omega^h_{\xi D}, \partial\Omega^h_{\xi N}$	=	approximated modelling boundaries where Dirichlet and Neumann boundary conditions are enforced
$\partial\Omega^i_{\xi I}$	=	i-th interface between two mesh elements
$\partial\Omega^h_{\xi I}$	=	set of inter-element interfaces
$\boldsymbol{\nu}^e$	=	elements unit normal
μ	=	penalty parameter
$\Pi_\xi, \partial\Pi_\xi$	=	background rectangle domain and boundary
φ	=	level-set function
E_i	=	i-th Young's modulus
ν_{ij}	=	ij-th Poisson's ratio
G_{ij}	=	ij-th shear modulus
E_r	=	reference Young's modulus
$\delta^0, \varepsilon^0, \sigma^0$	=	reference displacement, strain and stress
$\overline{N}_{cr}$	=	critical buckling load
$\overline{u}_{cr}$	=	critical displacement at buckling

II. Introduction

Nowadays, composite structures are widely employed in aerospace, automotive and naval engineering as high-performance structural components. With respect to their metallic counterparts, composite multilayered structures offer the engineers a wider set of design parameters, ranging from the stacking sequence of the whole laminate to the materials of the fibers and the matrix of the single layer. As a result, composite structures are able to achieve strength-to-weight and stiffness-to-weight ratios superior to those of metallic structures. However, because of the inherent heterogeneous nature, composite structures are characterized by a more complex distribution of strains and stresses.

Among various loading configurations, loads inducing compressive stress states are of crucial importance because they can drive thin and slender structures to sudden changes in their geometry and failure at loads level dramatically lower than those predicted by linear static analyses. These critical loads, known as buckling loads, depend on the properties and the geometry of the structure and, in multilayered shells, are strongly affected by the interplay between the curved geometry, the dissimilar materials and the possible presence of cutouts. Therefore, to safely employ composite structures as load-carrying components, tools able to accurately address the buckling problem of multilayered shells are of great engineering interest.

One approach to evaluating the buckling loads of a thin structure and thus the corresponding change in its geometry is to solve the equations of finite-strain elasticity, whereby the load-deformation response of the structure is generally computed via an iterative-incremental non-linear analysis, see e.g. [1–5]. Alternatively, buckling loads may be evaluated using the so-called bifurcation theory, which, given an initial equilibrium configuration, is based on seeking at least one additional distinct equilibrium solution in the neighborhood of the initial equilibrium state [6]. When the initial configuration is computed from a linear elastic analysis, the bifurcation approach is also known as the Euler's method and reduces to solving a linear eigenvalue problem, where the smallest eigenvalue denotes the multiplicative factor to be applied to the external loads in order for the structure to buckle and the corresponding eigenvector represents the buckled shape. The Euler's method is based on a linearized analysis and loses the information regarding the equilibrium path of the structure in the non-linear regime. However, it may be more efficient than solving the non-linear equations of elasticity, especially during the design

phase of structural components.

The composite multilayered shell problem, including the buckling analysis, is typically formulated using two-dimensional shell theories, which are based on suitable assumptions on the behavior of the involved mechanical fields through the shell thickness and reduction of the computational complexity of three-dimensional models. The most widely employed shell theories are the Classical Laminated Theory (CLT) and the First-order Shear Deformation Theory (FSDT), which rely on a linear through-the-thickness approximation of the displacement field and have been successfully employed for solving the linear buckling problem of plates and shells [7–10]. However, to obtain a more detailed resolution of the displacement, strain and stress distribution at the layers' level, researchers have enriched the through-the-thickness assumptions and introduced the so-called higher-order theories. These theories can broadly be classified into Equivalent Single Layer (ESL) theories [11–13], whereby the shell is replaced by a single layer having equivalent mechanical properties, and Layer-Wise theories [14, 15] where each layer is modelled independently and suitable interface conditions must be enforced. Combined approaches, such the sub-laminate theory [16], have also been proposed but are less common. A unified description of high-order theories for plates and shells has been introduced by Carrera through the Carrera Unified Formulation (CUF) [17, 18], which provides a framework for a systematic assessment of multiple structural theories.

In general, regardless of the chosen shell theory, the solution of the buckling problem requires numerical methods, especially when one considers the complex stress distribution that is typical of practical engineering applications. The most widely employed numerical method is the Finite Element Method (FEM), which is at the base of many commercial software libraries featuring a buckling solver and is still employed in current research studies focused on buckling analysis, see e.g. [19, 20].

Various numerical approaches have also been proposed as an alternative to the FEM with the aim to facilitate the use of high-order elements, non conformal meshes and/or enriched spaces of basis functions. Recent examples include the works by Thai et al.[21] and by Alesadi et al.[22, 23], who employed the Isogeometric Analysis (IGA) for solving the buckling problem of laminated plates modelled by the FSDT and by high-order theories, respectively; the IGA approach was also used by Gou et al.[24] for the stability analysis of thin shells and by Faroughi et al.[25], who investigated anisotropic solid-like composite shells. The use of an enriched approximation space can be found in the works by Nasirmanesh et al. [26, 27], who studied the buckling problem of cracked single-layer composite plates and functionally graded cylindrical shells via the extended finite element method (XFEM), and by Milazzo et al.[28–30], who proposed an extended Ritz (X-Ritz) approach based on the use of high-order crack functions to augment the space of polynomial basis functions for the buckling analysis of composite plate and plate assemblies modelled by the FSDT. The Ritz method was also employed by Sciascia et al.[31, 32] for the free-vibration and dynamic analysis of prestressed variable stiffness shells using the FSDT and by Vescovini et al [33, 34] for the buckling analysis of reinforced and highly anisotropic plates using higher-order kinematics. A common result in the aforementioned studies is the benefit of using higher-order and/or enriched basis function spaces in structural analysis.

The discontinuous Galerkin (DG) method has also proved a powerful and flexible technique for high-order accurate numerical modelling. The main features of a DG formulation are the representation of the approximate solution in a space of discontinuous basis functions and the introduction of suitably defined boundary integrals, which ensure the continuity of the solution at the inter-element interfaces and enforce the boundary conditions in terms of both prescribed displacement and traction fields. This allows the DG method to naturally handle arbitrarily-shaped elements while maintaining the high-order accuracy and to be seamlessly employed in combination with variable-order approximation spaces. The DG method has been successfully employed for the static analysis of plates and shell structures modelled via the CLT [35–37] and the FSDT [38, 39]. More recently, it has also been used to solve the governing equations of static elasticity and piezoelectricity associated with ESL [40–42] and LW [43–45] theories for multilayered plates and shells.

In the context of eigenvalue problems, the DG method has been used to solve the Laplace eigenproblem [46, 47], to compute the eigenfrequencies of the Maxwell equations in a cavity [48–50] and to study the hydrodynamic stability associated with the incompressible Navier–Stokes equations [51, 52]. However, to the best of the author knowledge, the application of the DG method to the eigenvalue problem associated with the linear buckling analysis of laminated plates and shells has not been investigated in the literature.

In this work, a novel DG-based formulation for the buckling analysis of composite multilayered structures modelled via general high-order theories is presented. The starting point of the formulation is the use of ESL theories for multilayered structures, whereby the through-the-thickness expansion is assumed for the covariant components of the displacement field. The corresponding buckling variational statement is derived using the Euler's method under the assumption that the structure is subjected to an initial stress distribution. The initial stress distribution is either prescribed or obtained from a linear elastic static analysis. Both the static and the buckling problems are solved via the Interior Penalty DG formulation previously introduced for the static behavior of composite structures, see Refs.[40–43]. In particular, we verify that, by introducing the domain terms accounting for the initial stress distribution and retaining the same boundary integrals employed in the static analyses to enforce the inter-element continuity and the boundary conditions, the present DG formulation provides a high-order accurate solution of the buckling problem for laminated plates and shells. Additionally, to account for the presence of cutouts, we employ the implicitly-defined mesh technique, whereby the mesh of the shell modelling domain is constructed by combining a background grid and an implicit representation of the cutout via a level set function. This strategy simplifies the meshing phase, whilst the flexibility of the DG method and the use of high-order quadrature rules for implicitly-defined domains and boundaries [53] ensure that the present formulation retains its high-order accuracy also in the presence of cutouts.

The paper is organized as follows: Sec.(III) introduces the linear buckling problem for multilayered shells; the linear static problem is also briefly recalled as it is employed to evaluate the initial stress distribution in the considered structures. Sec.(IV) presents the proposed Interior Penalty DG formulation for the solution of the considered static and buckling problems and discusses the meshing of the shell modelling domain via the implicitly-defined mesh technique. In Sec.(V), several numerical tests are performed for multilayered plates and shells without cutouts and for a multilayered plate with a circular cutout. The obtained results are compared with benchmarks taken from the literature or obtained with finite-element analyses. The final remarks to the work are given in Sec.(VI).

III. Problem formulation

We consider a multilayered shell occupying the volume $V \subset \mathbb{R}^3$, with boundary ∂V, and consisting of a stacking of N_ℓ layers. The layers are assumed homogeneous, orthotropic and perfectly-bonded at the layers' interfaces. The layers have thickness $\tau^{\langle \ell \rangle}$, with $\ell = 1, \dots, N_\ell$, such that the total thickness of the shell is $\tau = \sum_{\ell=1}^{N_\ell} \tau^{\langle \ell \rangle}$. The ℓ-th layer is also characterized by an orientation angle $\theta^{\langle \ell \rangle}$, which affects its constitutive behavior as detailed in Sec.(III.D). Throughout the paper, all quantities associated with the ℓ-th layer are denoted by the superscript $\langle \ell \rangle$.

A. Geometry description

The shell geometry is defined starting from the definition of the shell mean surface S, which is represented by the map

$$\boldsymbol{x}_0 = \boldsymbol{x}_0(\xi_1, \xi_2), \quad \text{for } (\xi_1, \xi_2) \in \Omega_\xi. \tag{1}$$

In Eq.(1), $\boldsymbol{x}_0 = (x_{01}, x_{02}, x_{03})^\intercal$ is a generic point on S and is given as a function of the curvilinear coordinates (ξ_1, ξ_2) that span the shell modelling domain $\Omega_\xi \subset \mathbb{R}^2$. Associated with each point on the mean surface is the normal unit vector $\boldsymbol{n}_0$, which is obtained from Eq.(1) as

$$\boldsymbol{n}_0 \equiv \frac{\boldsymbol{a}_1 \times \boldsymbol{a}_2}{||\boldsymbol{a}_1 \times \boldsymbol{a}_2||}, \tag{2}$$

where

$$\boldsymbol{a}_1 \equiv \frac{\partial \boldsymbol{x}_0}{\partial \xi_1} \quad \text{and} \quad \boldsymbol{a}_2 \equiv \frac{\partial \boldsymbol{x}_0}{\partial \xi_2}. \tag{3}$$

Let us now introduce a third curvilinear variable ξ_3 spanning the thickness interval $I_{\xi_3} \equiv [-\tau/2, \tau/2]$. Then, a generic point $\boldsymbol{x}$ of the shell volume V is given by the map

$$\boldsymbol{x} = \boldsymbol{x}(\xi_1, \xi_2, \xi_3) \equiv \boldsymbol{x}_0(\xi_1, \xi_2) + \xi_3 \boldsymbol{n}_0(\xi_1, \xi_2), \quad \text{for } (\xi_1, \xi_2, \xi_3) \in \Omega_\xi \times I_{\xi_3}. \tag{4}$$

Using Eq.(4), one introduces the local *covariant basis*, whose i-th vector is defined as $\boldsymbol{g}_i \equiv \partial \boldsymbol{x} / \partial \xi_i$, and the local *contravariant basis*, whose i-th vector $\boldsymbol{g}^i$ is defined such that $\boldsymbol{g}^i \cdot \boldsymbol{g}_j = \delta^i_j$, being δ^i_j the the Kronecker delta. The bases allow expressing the transformation between the Cartesian and the curvilinear coordinates systems. In particular, let (v_1, v_2, v_3) denote the Cartesian components of a generic vector in $\mathbb{R}^3$ and $(v_{\xi_1}, v_{\xi_2}, v_{\xi_3})$ denote the corresponding curvilinear covariant components. Then, the two sets of coordinates are related as follows [54]

$$\boldsymbol{v} = \boldsymbol{R}_\xi \boldsymbol{v}_\xi, \tag{5}$$

where $\boldsymbol{v} \equiv (v_1, v_2, v_3)^\intercal$, $\boldsymbol{v}_\xi \equiv (v_{\xi_1}, v_{\xi_2}, v_{\xi_3})^\intercal$ and $\boldsymbol{R}_\xi$ is a 3×3 matrix whose columns are vectors of the contravariant basis. We also introduce the covariant components g_{ij} of the metric tensor as $g_{ij} \equiv \boldsymbol{g}_i \cdot \boldsymbol{g}_j$, the determinant g of g_{ij}, and the contravariant components g^{ij} of the metric tensor as $g^{ij} \equiv \boldsymbol{g}^i \cdot \boldsymbol{g}^j$.

Finally, the map given in Eq.(4) allows defining the geometry of the layers of the shells. The volume $V^{\langle \ell \rangle}$ of the ℓ-th layer is identified by Eq.(4) for $\xi_3 \in I^{\langle \ell \rangle}_{\xi_3} \equiv [\xi^{\langle \ell \rangle}_{3b}, \xi^{\langle \ell \rangle}_{3t}]$, where $\xi^{\langle \ell \rangle}_{3b}$ and $\xi^{\langle \ell \rangle}_{3t}$ are the values of the curvilinear coordinate ξ_3 that identify the ℓ-th layer's bottom surface and the top surface, respectively. Note that $\xi^{\langle \ell \rangle}_{3t} - \xi^{\langle \ell \rangle}_{3b} = \tau^{\langle \ell \rangle}$ and that the layers are stacked such that $\xi^{\langle \ell - 1 \rangle}_{3t} = \xi^{\langle \ell \rangle}_{3b}$ for $\ell = 2, \dots, N_\ell$.

B. The Equivalent-Single-Layer theory for shells

Among the higher-order theories for multilayered shells, the formulation considered in this work is based on the displacement-based Equivalent-Single-Layer theory, see e.g.[17, 55], whereby the shell is replaced by a single mechanical layer with equivalent mechanical properties and all mechanical quantities are expressed in terms of displacement degrees of freedom. Let us introduce the vector $\boldsymbol{u} \equiv (u_1, u_2, u_3)^\intercal$ containing the Cartesian components of the displacement field and the vector $\boldsymbol{u}_\xi \equiv (u_{\xi_1}, u_{\xi_2}, u_{\xi_3})^\intercal$ containing the corresponding covariant components, which are related to $\boldsymbol{u}$ via Eq.(5). Then, following Guarino et al.[41, 42], we assume the following through-the-thickness expansion for the covariant component u_{ξ_i}

$$u_{\xi_i}(\xi_1, \xi_2, \xi_3) = \sum_{k=0}^{N_i} Z^i_k(\xi_3) U^i_k(\xi_1, \xi_2), \tag{6}$$

where $Z^i_k(\xi_3)$ is the k-th known thickness function, $U^i_k(\xi_1, \xi_2)$ is k-th unknown generalized displacement function and N_i represents the order of the expansion associated with u_{ξ_i}. Upon collecting the generalized displacements in the N_U-dimensional vector $\boldsymbol{U}$, with $N_U = N_1 + N_2 + N_3 + 3$, the expression given in Eq.(6) can be written in compact form as

$$\boldsymbol{u}_\xi = \boldsymbol{Z}(\xi_3) \boldsymbol{U}(\xi_1, \xi_2), \tag{7}$$

where $\boldsymbol{Z}$ is a $3 \times N_U$ matrix containing the thickness functions suitably ordered to be consistent with the ordering of $\boldsymbol{U}$. Note that the present approach allows selecting the order of expansion independently for each displacement component. For instance, the FSDT would

be obtained by setting $N_1 = N_2 = 1$, $N_3 = 0$, $Z_0^1(\xi_3) = Z_0^2(\xi_3) = Z_0^3(\xi_3) = 1$ and $Z_1^1(\xi_3) = Z_1^2(\xi_3) = \xi_3$, such that the matrix $\boldsymbol{Z}$ may be

$$\boldsymbol{Z}(\xi_3) = \begin{bmatrix} 1 & 0 & 0 & \xi_3 & 0 \\ 0 & 1 & 0 & 0 & \xi_3 \\ 0 & 0 & 1 & 0 & 0 \end{bmatrix}. \tag{8}$$

In the next sections, the strain and the stress components will be written in terms of the generalized displacement vector $\boldsymbol{U}$ and its derivatives with respect to ξ_1 and ξ_2.

C. Strain-displacement relations

The relationship between the displacement field and the strain field considered here is based on the small-strain assumption. Following Gulizzi et al.[40, 43] and using the Voigt notation, the vector $\boldsymbol{\gamma}$ containing the Cartesian engineering strain components, i.e. $\boldsymbol{\gamma} = (\gamma_{11}, \gamma_{22}, \gamma_{33}, \gamma_{23}, \gamma_{13}, \gamma_{12})^\intercal$, is written in terms of the displacement vector $\boldsymbol{u}$ as

$$\boldsymbol{\gamma} = \boldsymbol{I}_i \frac{\partial \boldsymbol{u}}{\partial x_i}, \tag{9}$$

where the following 6×3 matrices have been introduced

$$\boldsymbol{I}_1 \equiv \begin{bmatrix} 1 & 0 & 0 \\ 0 & 0 & 0 \\ 0 & 0 & 0 \\ 0 & 0 & 0 \\ 0 & 0 & 1 \\ 0 & 1 & 0 \end{bmatrix}, \quad \boldsymbol{I}_2 \equiv \begin{bmatrix} 0 & 0 & 0 \\ 0 & 1 & 0 \\ 0 & 0 & 0 \\ 0 & 0 & 1 \\ 0 & 0 & 0 \\ 1 & 0 & 0 \end{bmatrix} \quad \text{and} \quad \boldsymbol{I}_3 \equiv \begin{bmatrix} 0 & 0 & 0 \\ 0 & 0 & 0 \\ 0 & 0 & 1 \\ 0 & 1 & 0 \\ 1 & 0 & 0 \\ 0 & 0 & 0 \end{bmatrix}. \tag{10}$$

In Eq.(9) and in the remainder of the paper, the Einstein summation convection is employed with Latin indices spanning the set $\{1, 2, 3\}$ and Greek indices spanning the set $\{1, 2\}$.

To express the vector $\boldsymbol{\gamma}$ in terms of the generalized displacement vector $\boldsymbol{U}$ and its derivatives with respect to ξ_α, with $\alpha = 1, 2$, we first use Eqs.(5) and (7) and write the derivatives appearing in Eq.(9) as follows

$$\frac{\partial \boldsymbol{u}}{\partial x_i} = \boldsymbol{D}_{0i}\boldsymbol{U} + \boldsymbol{D}_{\alpha i}\frac{\partial \boldsymbol{U}}{\partial \xi_\alpha}, \tag{11}$$

where

$$\boldsymbol{D}_{0i} \equiv \frac{\partial \xi_j}{\partial x_i}\frac{\partial \boldsymbol{R}_\xi}{\partial \xi_j}\boldsymbol{Z} + \frac{\partial \xi_3}{\partial x_i}\boldsymbol{R}_\xi \frac{\mathrm{d}\boldsymbol{Z}}{\mathrm{d}\xi_3}, \quad \text{and} \quad \boldsymbol{D}_{\alpha i} \equiv \frac{\partial \xi_\alpha}{\partial x_i}\boldsymbol{R}_\xi \boldsymbol{Z}. \tag{12}$$

Then, upon substituting Eq.(11) into Eq.(9), one obtains

$$\boldsymbol{\gamma} = \boldsymbol{J}_0\boldsymbol{U} + \boldsymbol{J}_\alpha \frac{\partial \boldsymbol{U}}{\partial \xi_\alpha}, \tag{13}$$

where

$$\boldsymbol{J}_0 \equiv \boldsymbol{I}_i\boldsymbol{D}_{0i} \quad \text{and} \quad \boldsymbol{J}_\alpha \equiv \boldsymbol{I}_i\boldsymbol{D}_{\alpha i}. \tag{14}$$

To conclude this section, it is worth noting that Eqs.(7) and (13) have been introduced without using the superscript $\langle \ell \rangle$ or mentioning the stacking sequence of the shell. In fact, Eqs.(7) and (13) are valid throughout the shell thickness and for each layer of the shell. This is typical of ESL formulations and has the advantage that the continuity of the displacement field at the interface between consecutive layers is automatically satisfied.

D. Constitutive behavior

The constitutive behavior of the multilayered shell is determined starting from the constitutive behavior of its layers, which are assumed linear elastic. For a generic point $\boldsymbol{x} \in V^{\langle \ell \rangle}$, we introduce a local reference system, identified by the unit vectors $\boldsymbol{m}_1^{\langle \ell \rangle}$, $\boldsymbol{m}_2^{\langle \ell \rangle}$ and $\boldsymbol{m}_3^{\langle \ell \rangle}$, such that the constitutive behavior of the ℓ-th layer may be assumed orthotropic. The vectors of the local reference system are defined as follows

$$\boldsymbol{m}_1^{\langle \ell \rangle} \equiv \boldsymbol{R}_{\boldsymbol{n}_0}(\theta^{\langle \ell \rangle})\frac{\boldsymbol{g}_1}{||\boldsymbol{g}_1||}, \quad \boldsymbol{m}_3^{\langle \ell \rangle} \equiv \boldsymbol{n}_0, \quad \text{and} \quad \boldsymbol{m}_2^{\langle \ell \rangle} \equiv \boldsymbol{m}_3^{\langle \ell \rangle} \times \boldsymbol{m}_1^{\langle \ell \rangle}, \tag{15}$$

where $\boldsymbol{R}_{\boldsymbol{n}_0}(\theta^{\langle \ell \rangle})$ is a 3×3 matrix that performs a rotation of the lamination angle $\theta^{\langle \ell \rangle}$ around the normal vector $\boldsymbol{n}_0$. It is worth pointing out that this choice of the layers' local reference system does not represent a restriction for the proposed formulation. In fact, the formulation allows defining the vector $\boldsymbol{m}_1^{\langle \ell \rangle}$ in different reference systems. For example, the vector $\boldsymbol{m}_1^{\langle \ell \rangle}$ may be defined with respect to a unit vector

in the global Cartesian reference system; this strategy has been tested in Ref.[41] and allows the modelling of multilayered plates where the layers are characterized by parallel straight fibers but the vectors of the curvilinear basis change as functions of ξ_1 and ξ_2. Other choices of the layers' local reference systems may also be employed, such that those stemming from the intersection of the shell surface with a given plane, see e.g. [56], but they will not be considered here. Within the linear elasticity hypothesis, the stress-strain relationship in the local reference system is written as

$$\widetilde{\boldsymbol{\sigma}}^{\langle\ell\rangle} = \widetilde{\boldsymbol{c}}^{\langle\ell\rangle}\widetilde{\boldsymbol{\gamma}}^{\langle\ell\rangle}, \tag{16}$$

where $\widetilde{\boldsymbol{\gamma}}^{\langle\ell\rangle}$ and $\widetilde{\boldsymbol{\sigma}}^{\langle\ell\rangle}$ are 6-dimensional vectors containing the strain components and stress components, respectively, in Voigt notation, and $\widetilde{\boldsymbol{c}}^{\langle\ell\rangle}$ is the corresponding stiffness matrix in the local reference system, which is given in terms of the engineering constants as described in [57]. Using standard transformation procedures, see e.g.[57, 58], Eq.(16) is written in the global reference system as

$$\boldsymbol{\sigma}^{\langle\ell\rangle} = \boldsymbol{c}^{\langle\ell\rangle}\boldsymbol{\gamma}. \tag{17}$$

Note that in Eq.(17) the superscript $\langle\ell\rangle$ does not appear on the vector $\boldsymbol{\gamma}$ containing the engineering strain components in the global reference system because it is assumed that $\boldsymbol{\gamma}$ is given by Eq.(13). In fact, upon substituting Eq.(13) into Eq.(17), the vector $\boldsymbol{\sigma}^{\langle\ell\rangle}$ containing the stress components in the global reference system is expressed in terms of the generalized displacement vector $\boldsymbol{U}$ and its derivatives as

$$\boldsymbol{\sigma}^{\langle\ell\rangle} = \boldsymbol{c}^{\langle\ell\rangle}\left(\boldsymbol{J}_0\boldsymbol{U} + \boldsymbol{J}_\alpha\frac{\partial\boldsymbol{U}}{\partial\xi_\alpha}\right), \quad \text{for} \quad \ell = 1,\dots,N_\ell. \tag{18}$$

As detailed in the next two sections, it is now possible to express the static and the buckling problems of multilayered shells modelled via ESL theories in terms of the vector $\boldsymbol{U}$.

E. Static problem

In the Cartesian global reference system, the static response of multilayered composite shells subjected to body forces $\overline{\boldsymbol{b}}$ and boundary tractions $\overline{\boldsymbol{t}}$ is derived from the three-dimensional principle of virtual displacements, which reads

$$\sum_{\ell=1}^{N_\ell}\int_{V^{\langle\ell\rangle}}\delta\boldsymbol{\gamma}^\top\boldsymbol{\sigma}^{\langle\ell\rangle}\,\mathrm{d}V = \int_V\delta\boldsymbol{u}^\top\overline{\boldsymbol{b}}\,\mathrm{d}V + \int_{\partial V}\delta\boldsymbol{u}^\top\overline{\boldsymbol{t}}\,\mathrm{d}\partial V, \tag{19}$$

where $\delta\bullet$ denotes the variation of $\bullet$ and, consistently with ESL theories, it was implicitly assumed that the displacement and the strain fields do not depend on the layer ℓ. Upon substituting Eqs.(7), (13) and (18) into Eq.(19), one obtains the following variational statement for the static analysis of a multilayered shell

$$\int_{\Omega_\xi}\left[\frac{\partial\delta\boldsymbol{U}^\top}{\partial\xi_\alpha}\left(\boldsymbol{Q}_{\alpha\beta}\frac{\partial\boldsymbol{U}}{\partial\xi_\beta} + \boldsymbol{R}_{\alpha3}\boldsymbol{U}\right) + \delta\boldsymbol{U}^\top\left(\boldsymbol{R}_{\alpha3}^\top\frac{\partial\boldsymbol{U}}{\partial\xi_\alpha} + \boldsymbol{S}_{33}\boldsymbol{U}\right)\right]\mathrm{d}\Omega_\xi = \int_{\Omega_\xi}\delta\boldsymbol{U}^\top\overline{\boldsymbol{B}}\,\mathrm{d}\Omega_\xi + \int_{\partial\Omega_\xi}\delta\boldsymbol{U}^\top\overline{\boldsymbol{T}}\,\mathrm{d}\partial\Omega_\xi, \tag{20}$$

which is written only in terms of the generalized displacement vector $\boldsymbol{U}$. In Eq.(20), the matrices $\boldsymbol{Q}_{\alpha\beta}$, $\boldsymbol{R}_{\alpha3}$, and $\boldsymbol{S}_{33}$ are referred to as generalized stiffness matrices and are given as follows

$$\boldsymbol{Q}_{\alpha\beta} \equiv \sum_{\ell=1}^{N_\ell}\int_{\xi_{3b}^{\langle\ell\rangle}}^{\xi_{3t}^{\langle\ell\rangle}}\boldsymbol{J}_\alpha^\top\boldsymbol{c}^{\langle\ell\rangle}\boldsymbol{J}_\beta\sqrt{g}\,\mathrm{d}\xi_3, \tag{21a}$$

$$\boldsymbol{R}_{\alpha3} \equiv \sum_{\ell=1}^{N_\ell}\int_{\xi_{3b}^{\langle\ell\rangle}}^{\xi_{3t}^{\langle\ell\rangle}}\boldsymbol{J}_\alpha^\top\boldsymbol{c}^{\langle\ell\rangle}\boldsymbol{J}_0\sqrt{g}\,\mathrm{d}\xi_3, \tag{21b}$$

$$\boldsymbol{S}_{33} \equiv \sum_{\ell=1}^{N_\ell}\int_{\xi_{3b}^{\langle\ell\rangle}}^{\xi_{3t}^{\langle\ell\rangle}}\boldsymbol{J}_0^\top\boldsymbol{c}^{\langle\ell\rangle}\boldsymbol{J}_0\sqrt{g}\,\mathrm{d}\xi_3. \tag{21c}$$

Similarly, the generalized volume loads $\overline{\boldsymbol{B}}$ and the generalized boundary loads $\overline{\boldsymbol{T}}$ are given as

$$\overline{\boldsymbol{B}} \equiv \left(\boldsymbol{Z}^\top\boldsymbol{R}_\xi^\top\overline{\boldsymbol{t}}\sqrt{g}\sqrt{n_i g^{ij} n_j}\right)_{\xi_3=\pm\tau/2} + \int_{-\tau/2}^{\tau/2}\boldsymbol{Z}^\top\boldsymbol{R}_\xi^\top\overline{\boldsymbol{b}}\sqrt{g}\,\mathrm{d}\xi_3, \tag{22a}$$

and

$$\overline{\boldsymbol{T}} \equiv \int_{-\tau/2}^{\tau/2}\boldsymbol{Z}^\top\boldsymbol{R}_\xi^\top\overline{\boldsymbol{t}}\sqrt{g}\sqrt{n_i g^{ij} n_j}\,\mathrm{d}\xi_3. \tag{22b}$$

It is worth pointing out that the integrals over $V^{\langle\ell\rangle}$ and $\partial V^{\langle\ell\rangle}$ in Eq.(19) have been transformed into integrals over Ω_ξ and $\partial\Omega_\xi$ using the relationships $\mathrm{d}V = \sqrt{g}\,\mathrm{d}\Omega\,\mathrm{d}\xi_3$, $\mathrm{d}\partial V = \sqrt{g}\sqrt{n_i g^{ij} n_j}\,\mathrm{d}\Omega_\xi$ for the top and bottom surfaces of the shell and $\mathrm{d}\partial V = \sqrt{g}\sqrt{n_i g^{ij} n_j}\,\mathrm{d}\partial\Omega\,\mathrm{d}\xi_3$ for the lateral surface of the shell, where n_i is the i-th Cartesian component of the outer unit normal at $\boldsymbol{x} \in \partial V$, see [54]. Additionally, we note that the set of partial differential equations governing the statics of multilayered shells can be derived from Eq.(20) by applying standard integration by parts and recalling that Eq.(20) must be valid for any $\delta\boldsymbol{U}$. However, for the sake of conciseness, the strong form of governing equations is not reported here and may be found in Refs.[40–43].

F. Buckling problem

A similar derivation to the one presented in the preceding section may be followed to obtain the variational statement of linear buckling problem. We start from the three-dimensional variational statement of the Eulerian buckling [6], which is written as

$$\sum_{\ell=1}^{N_\ell} \int_{V^{\langle\ell\rangle}} \delta\boldsymbol{\gamma}^\intercal \boldsymbol{\sigma}^{\langle\ell\rangle} \mathrm{d}V + \lambda \sum_{\ell=1}^{N_\ell} \int_{V^{\langle\ell\rangle}} \overline{\sigma}_{ij}^{\langle\ell\rangle} \frac{\partial \delta \boldsymbol{u}^\intercal}{\partial x_i} \frac{\partial \boldsymbol{u}}{\partial x_j} \mathrm{d}V = 0, \tag{23}$$

where $\overline{\sigma}_{ij}^{\langle\ell\rangle}$ is the ij-th component of the initial stress field, the vectors $\boldsymbol{u}$, $\boldsymbol{\gamma}$ and $\boldsymbol{\sigma}^{\langle\ell\rangle}$ are the displacement, strain and stress fields, respectively, of the additional adjacent equilibrium configuration, and λ is the eigenvalue of the buckling problem. Note that the vectors $\boldsymbol{u}$, $\boldsymbol{\gamma}$ and $\boldsymbol{\sigma}^{\langle\ell\rangle}$ represent the eigenfunction associated with the eigenvector λ and have a different meaning than the vectors appearing in Eq.(19). Eventually, the smallest value of λ represents the critical multiplicative factor to be applied to the external loads in order for the structure to buckle.

The buckling problem is then expressed only in terms of the adjacent configuration of the generalized displacement vector $\boldsymbol{U}$ by substituting Eqs.(7), (13) and (18) into Eq.(23) to obtain

$$\int_{\Omega_\xi} \left[\frac{\partial \delta \boldsymbol{U}^\intercal}{\partial \xi_\alpha} \left(\boldsymbol{Q}_{\alpha\beta} \frac{\partial \boldsymbol{U}}{\partial \xi_\beta} + \boldsymbol{R}_{\alpha 3} \boldsymbol{U} \right) + \delta \boldsymbol{U}^\intercal \left(\boldsymbol{R}_{\alpha 3}^\intercal \frac{\partial \boldsymbol{U}}{\partial \xi_\alpha} + \boldsymbol{S}_{33} \boldsymbol{U} \right) \right] \mathrm{d}\Omega_\xi + \lambda \int_{\Omega_\xi} \left[\frac{\partial \delta \boldsymbol{U}^\intercal}{\partial \xi_\alpha} \left(\boldsymbol{Q}^G_{\alpha\beta} \frac{\partial \boldsymbol{U}}{\partial \xi_\beta} + \boldsymbol{R}^G_{\alpha 3} \boldsymbol{U} \right) + \delta \boldsymbol{U}^\intercal \left(\boldsymbol{R}^{G\intercal}_{\alpha 3} \frac{\partial \boldsymbol{U}}{\partial \xi_\alpha} + \boldsymbol{S}^G_{33} \boldsymbol{U} \right) \right] \mathrm{d}\Omega_\xi = 0, \tag{24}$$

where the matrices $\boldsymbol{Q}_{\alpha\beta}$, $\boldsymbol{R}_{\alpha 3}$, and $\boldsymbol{S}_{33}$ have the same meaning of those appearing in Eq.(20) and are given in Eq.(21), while the matrices $\boldsymbol{Q}^G_{\alpha\beta}$, $\boldsymbol{R}^G_{\alpha 3}$, and $\boldsymbol{S}^G_{33}$ represent the generalized geometric stiffness matrices and are defined as follows

$$\boldsymbol{Q}^G_{\alpha\beta} \equiv \sum_{\ell=1}^{N_\ell} \int_{\xi_{3b}^{\langle\ell\rangle}}^{\xi_{3t}^{\langle\ell\rangle}} \boldsymbol{D}_{\alpha i}^\intercal \overline{\sigma}_{ij}^{\langle\ell\rangle} \boldsymbol{D}_{\beta j} \sqrt{g}\, \mathrm{d}\xi_3, \tag{25a}$$

$$\boldsymbol{R}^G_{\alpha 3} \equiv \sum_{\ell=1}^{N_\ell} \int_{\xi_{3b}^{\langle\ell\rangle}}^{\xi_{3t}^{\langle\ell\rangle}} \boldsymbol{D}_{\alpha i}^\intercal \overline{\sigma}_{ij}^{\langle\ell\rangle} \boldsymbol{D}_{0 j} \sqrt{g}\, \mathrm{d}\xi_3, \tag{25b}$$

$$\boldsymbol{S}^G_{33} \equiv \sum_{\ell=1}^{N_\ell} \int_{\xi_{3b}^{\langle\ell\rangle}}^{\xi_{3t}^{\langle\ell\rangle}} \boldsymbol{D}_{0 i}^\intercal \overline{\sigma}_{ij}^{\langle\ell\rangle} \boldsymbol{D}_{0 j} \sqrt{g}\, \mathrm{d}\xi_3. \tag{25c}$$

IV. Interior Penalty Discontinuous Galerkin formulation

In this section, we present the Interior Penalty discontinuous Galerkin formulation for the solution of the buckling problem discussed in Sec.(III.F). The original formulation for linear elastostatics of plates and shells [40–43] is first recalled as it may be used to compute the initial stress appearing in the definition of the generalized geometric stiffness matrices, see Eq.(25). Then, the formulation is extended to the buckling problem. However, prior to stating the DG formulation for Eqs.(20) and (24), it is worth introducing some of the quantities that are typical of DG approaches.

The DG method is a numerical technique based on a partition of the domain of analysis into a collection of non-overlapping elements. Upon noting that both Eqs.(20) and (24) are defined over the shell modelling domain Ω_ξ, let us introduce a mesh of Ω_ξ consisting of N_e elements, i.e. $\Omega_\xi \approx \Omega^h_\xi \equiv \bigcup_{e=1}^{N_e} \Omega^e_\xi$, being Ω^e_ξ the generic e-th mesh element. Let us also introduce the space $\mathcal{V}_{hp}$ of discontinuous basis functions as follows

$$\mathcal{V}_{hp} \equiv \left\{ v : \Omega^h_\xi \to \mathbb{R} \mid v|_{\Omega^e_\xi} \in \mathcal{P}^e_p \ \forall e = 1, ..., N_e \right\}, \tag{26}$$

where $\mathcal{P}^e_p$ denotes the space of polynomial functions of degree at most p defined over Ω^e_ξ. Consistently, the space of N-dimensional discontinuous vector field is defined as $\mathcal{V}^N_{hp} \equiv (\mathcal{V}_{hp})^N$.

The partition of Ω_ξ induces the discretization of the boundary $\partial\Omega_\xi$ of the shell modelling domain, i.e. $\partial\Omega_\xi \approx \partial\Omega^h_{\xi D} \cup \partial\Omega^h_{\xi N}$, where $\partial\Omega^h_{\xi D}$ denotes the collection of the element boundaries where Dirichlet boundary conditions are enforced, i.e. $\partial\Omega^h_{\xi D} \equiv \bigcup_{e=1}^{N_e} \partial\Omega^e_{\xi D}$, and $\partial\Omega^h_{\xi N}$ denotes the collection of the element boundaries where Neumann boundary conditions are enforced, i.e. $\partial\Omega^h_{\xi N} \equiv \bigcup_{e=1}^{N_e} \partial\Omega^e_{\xi N}$. Additionally, the partition of Ω_ξ introduces the set of inter-element interfaces $\partial\Omega^h_{\xi I} \equiv \bigcup_{i=1}^{N_i} \partial\Omega^i_{\xi I}$, where N_i is the total number of inter-element interfaces and $\partial\Omega^i_{\xi I}$ denotes the i-th interface between two generic elements e and e', that is $\partial\Omega^i_{\xi I} \equiv \Omega^e_\xi \cap \Omega^{e'}_\xi$. Figure (1) shows a sample 3×3 mesh of a square domain where a generic e-th element is highlighted in darker color; the figure also highlights the element's unit normal $\boldsymbol{\nu}^e = (\nu^e_1, \nu^e_2)$, its outer boundary $\partial\Omega^e_{\xi D} \cup \partial\Omega^e_{\xi N}$ and the interface $\partial\Omega^i_{\xi I}$ shared with its neighbor $\Omega^{e'}_\xi$. Finally, we introduce the following *average* and *jump* operators at the i-th interface

$$\{\bullet\}^i \equiv \frac{1}{2} \left(\bullet^e + \bullet^{e'} \right) \quad \text{and} \quad [[\bullet]]^i_\alpha \equiv \nu^e_\alpha \bullet^e + \nu^{e'}_\alpha \bullet^{e'}, \tag{27}$$

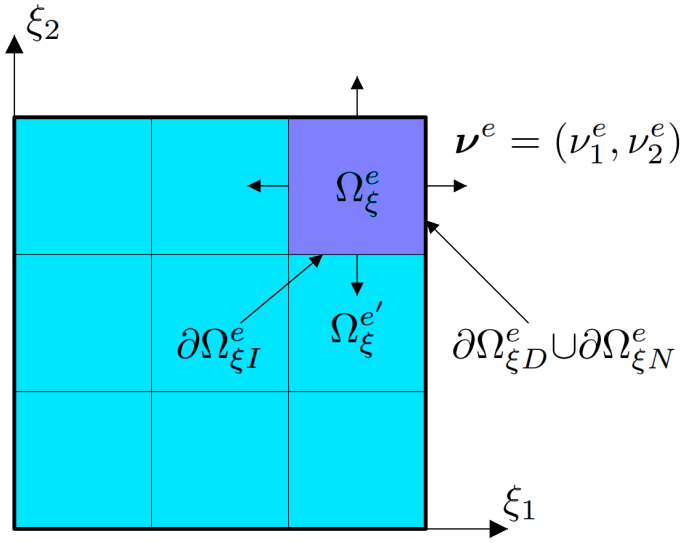

Fig. 1 Sample 3×3 mesh highlight a generic e-th element and its boundaries and outer unit normal.

and the so-called *broken integral*

$$\int_{\Omega_\xi^h} \bullet \equiv \sum_{e=1}^{N_e} \int_{\Omega_\xi^e} \bullet^e \, \mathrm{d}\Omega_\xi \tag{28a}$$

and

$$\int_{\partial\Omega_{\xi I}^h} \bullet \equiv \sum_{i=1}^{N_i} \int_{\partial\Omega_{\xi I}^i} \bullet^i \, \mathrm{d}\partial\Omega_\xi, \quad \int_{\partial\Omega_{\xi D}^h} \bullet \equiv \sum_{e=1}^{N_e} \int_{\partial\Omega_{\xi D}^e} \bullet^e \, \mathrm{d}\partial\Omega_\xi, \quad \int_{\partial\Omega_{\xi N}^h} \bullet \equiv \sum_{e=1}^{N_e} \int_{\partial\Omega_{\xi N}^e} \bullet^e \, \mathrm{d}\partial\Omega_\xi. \tag{28b}$$

A. Discontinuous Galerkin formulation for the static problem

Following Refs.[40–43], the Interior Penalty DG formulation for solving the static problem of multilayered plates and shells given in Eq.(20) can be stated as follows: find $\boldsymbol{U}_h \in \mathcal{V}_{hp}^{N_U}$ such that

$$B(\boldsymbol{V}, \boldsymbol{U}_h) = F(\boldsymbol{V}, \overline{\boldsymbol{B}}, \overline{\boldsymbol{T}}, \overline{\boldsymbol{U}}), \quad \forall \boldsymbol{V} \in \mathcal{V}_{hp}^{N_U}, \tag{29}$$

where

$$\begin{aligned} B(\boldsymbol{V}, \boldsymbol{U}_h) \equiv & \int_{\Omega_\xi^h} \frac{\partial \boldsymbol{V}^\intercal}{\partial \xi_\alpha} \left(\boldsymbol{Q}_{\alpha\beta} \frac{\partial \boldsymbol{U}_h}{\partial \xi_\beta} + \boldsymbol{R}_{\alpha 3} \boldsymbol{U}_h \right) + \boldsymbol{V}^\intercal \left(\boldsymbol{R}_{\alpha 3}^\intercal \frac{\partial \boldsymbol{U}_h}{\partial \xi_\alpha} + \boldsymbol{S}_{33} \boldsymbol{U}_h \right) + \\ & - \int_{\partial\Omega_{\xi I}^h} [\![\boldsymbol{V}]\!]_\alpha^\intercal \left\{ \boldsymbol{Q}_{\alpha\beta} \frac{\partial \boldsymbol{U}_h}{\partial \xi_\beta} + \boldsymbol{R}_{\alpha 3} \boldsymbol{U}_h \right\} + \left\{ \frac{\partial \boldsymbol{V}^\intercal}{\partial \xi_\alpha} \boldsymbol{Q}_{\alpha\beta} + \boldsymbol{V}^\intercal \boldsymbol{R}_{\beta 3}^\intercal \right\} [\![\boldsymbol{U}_h]\!]_\beta + \\ & - \int_{\partial\Omega_{\xi D}^h} \nu_\alpha \boldsymbol{V}^\intercal \left(\boldsymbol{Q}_{\alpha\beta} \frac{\partial \boldsymbol{U}_h}{\partial \xi_\beta} + \boldsymbol{R}_{\alpha 3} \boldsymbol{U}_h \right) + \left(\frac{\partial \boldsymbol{V}^\intercal}{\partial \xi_\alpha} \boldsymbol{Q}_{\alpha\beta} + \boldsymbol{V}^\intercal \boldsymbol{R}_{\beta 3}^\intercal \right) \boldsymbol{U}_h \nu_\beta + \\ & + \int_{\partial\Omega_{\xi I}^h} \mu [\![\boldsymbol{V}]\!]_\alpha^\intercal [\![\boldsymbol{U}_h]\!]_\alpha + \int_{\partial\Omega_{\xi D}^h} \mu \boldsymbol{V}^\intercal \boldsymbol{U}_h, \quad \text{and} \end{aligned} \tag{30}$$

and

$$F(\boldsymbol{V}, \overline{\boldsymbol{B}}, \overline{\boldsymbol{T}}, \overline{\boldsymbol{U}}) \equiv \int_{\Omega_\xi^h} \boldsymbol{V}^\intercal \overline{\boldsymbol{B}} + \int_{\partial\Omega_{\xi N}^h} \boldsymbol{V}^\intercal \overline{\boldsymbol{T}} - \int_{\partial\Omega_{\xi D}^h} \left(\frac{\partial \boldsymbol{V}^\intercal}{\partial \xi_\alpha} \boldsymbol{Q}_{\alpha\beta} + \boldsymbol{V}^\intercal \boldsymbol{R}_{\beta 3}^\intercal \right) \overline{\boldsymbol{U}} \nu_\beta + \int_{\partial\Omega_{\xi D}^h} \mu \boldsymbol{V}^\intercal \overline{\boldsymbol{U}}. \tag{31}$$

By comparing Eq.(20) and (29), it is possible to notice the term $B(\boldsymbol{V}, \boldsymbol{U}_h)$ consists of the approximate version of left hand-side of Eq.(20), where Ω_ξ^h has replaced Ω_ξ and $\boldsymbol{V}$ has replaced $\delta\boldsymbol{U}$, and some additional boundary terms, which are defined over the boundaries $\partial\Omega_{\xi I}^h$ and $\partial\Omega_{\xi D}^h$ and are responsible for the continuity of the solution throughout the mesh elements and the enforcement of the boundary conditions. Similarly, the term $F(\boldsymbol{V}, \overline{\boldsymbol{B}}, \overline{\boldsymbol{T}}, \overline{\boldsymbol{U}})$ consists of the approximate version of the right hand-side of Eq.(20) and some additional boundary terms, which are defined over the boundary $\partial\Omega_{\xi D}^h$ and are function of the prescribed value $\overline{\boldsymbol{U}}$ of the generalized displacements. As a last comment, we note that Eqs.(30) and (31) contain the penalty term μ, which is an additional parameter of the formulation that must be suitably chosen. In particular, as common in Interior Penalty DG formulations, see e.g. [59], the value of μ is chosen as $\mu \sim Qh^{-1}$,

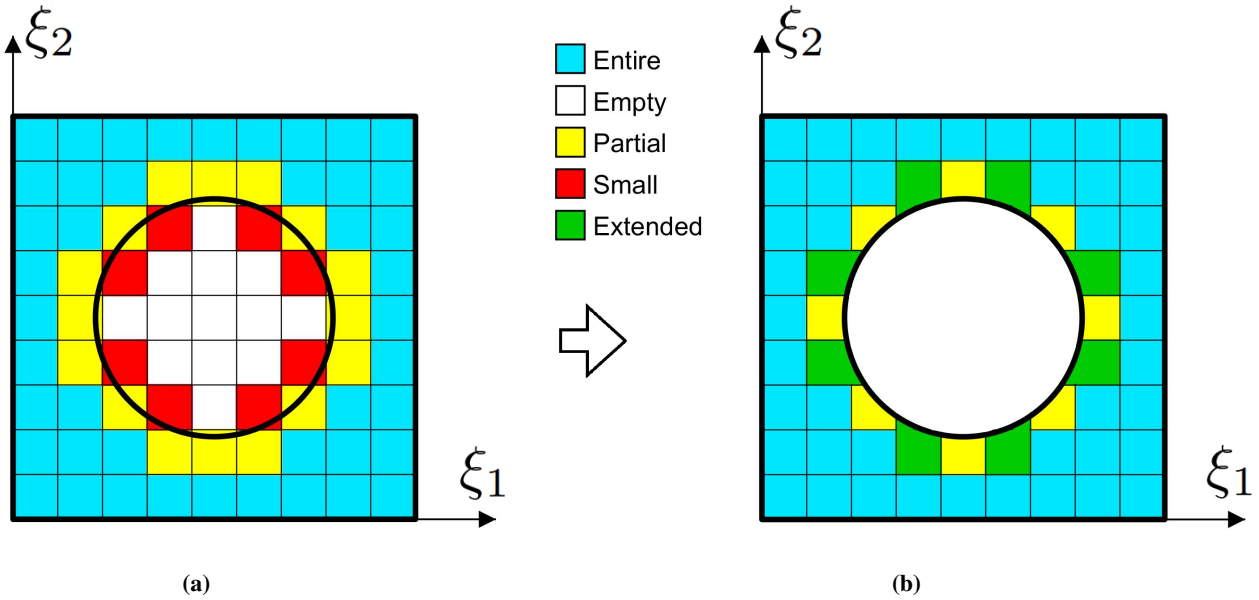

Fig. 2 (a) Cell classification according to their volume fraction. (b) Resulting implicitly-defined mesh after the cell-merging strategy.

where h is a characteristic mesh size and Q is a sufficiently large constant proportional to some significant stiffness of the shell section, e.g. the highest Young's modulus. The investigation conducted by Gulizzi et al.[40, 43] shows that choosing the penalty parameter as $\mu = 10^s E/h$, with $s \in [0, 4]$ and E being the largest Young's modulus of the layers' materials, does not affect the numerical results. As such, even for variable stiffness structures, stemming for instance from variable thickness and/or variable fiber orientation, it is reasonable to expect that the analysis can be conducted using a unique value of the penalty parameter, as the stiffness variation within such structures is usually limited to relatively small percentages. The use of a spatially variable penalty parameter may be beneficial to model structures with large mismatch in the material properties; however, these aspects go beyond the scope of the present work and will be considered in future studies.

B. Discontinuous Galerkin formulation for the buckling problem

The formulation proposed in this work for solving the linear buckling problem of multilayered shells is derived from the variational statement given in Eq.(24). In particular, it is stated as follow: find the eigenfunction $\boldsymbol{U}_h \in \mathcal{V}_{hp}^{N_U}$ and the eigenvalue λ_h such that

$$B(\boldsymbol{V}, \boldsymbol{U}_h) + \lambda_h B^G(\boldsymbol{V}, \boldsymbol{U}_h, \overline{\sigma}_{ij}) = 0, \quad \forall \boldsymbol{V} \in \mathcal{V}_{hp}^{N_U}, \tag{32}$$

where $B(\boldsymbol{V}, \boldsymbol{U}_h)$ is given in Eq.(30) and $B^G(\boldsymbol{V}, \boldsymbol{U}_h, \overline{\sigma}_{ij})$ is defined as

$$B^G(\boldsymbol{V}, \boldsymbol{U}_h, \overline{\sigma}_{ij}) \equiv \int_{\Omega_\xi^h} \frac{\partial \boldsymbol{V}^\intercal}{\partial \xi_\alpha} \left(\boldsymbol{Q}_{\alpha\beta}^G \frac{\partial \boldsymbol{U}_h}{\partial \xi_\beta} + \boldsymbol{R}_{\alpha 3}^G \boldsymbol{U}_h \right) + \boldsymbol{V}^\intercal \left(\boldsymbol{R}_{\alpha 3}^{G\intercal} \frac{\partial \boldsymbol{U}_h}{\partial \xi_\alpha} + \boldsymbol{S}_{33}^G \boldsymbol{U}_h \right). \tag{33}$$

The buckling DG formulation given in Eq.(32) employs the same bilinear form $B(\boldsymbol{V}, \boldsymbol{U}_h)$ introduced for the static DG formulation given in Eq.(29) including the boundary terms defined over $\partial\Omega_{\xi I}^h$ and $\partial\Omega_{\xi D}^h$. While it is clear that the boundary terms defined over $\partial\Omega_{\xi I}^h$ are needed to ensure the continuity of the solution among the mesh elements, it is worth noting that the boundary terms defined over $\partial\Omega_{\xi D}^h$ are also required because the adjacent solution $\boldsymbol{U}$ must verify $\boldsymbol{U} = \boldsymbol{0}$ on $\partial\Omega_{\xi D}$. On the other hand, the bilinear form $B^G(\boldsymbol{V}, \boldsymbol{U}_h, \overline{\sigma}_{ij})$ form consists of the approximate version of the second integral appearing in Eq.(24) without additional boundary terms. As show by the numerical tests discussed in Sec.(V), the DG formulation given in Eq.(32) provides the solution of the linear buckling problem for multilayered shells. It is work noting that, in Eq.(33), the penalty parameter appears only in the definition of $B(\boldsymbol{V}, \boldsymbol{U}_h)$ to enforce the inter-element continuity and the homogeneous boundary conditions, while it does not appear in the bilinear form $B^G(\boldsymbol{V}, \boldsymbol{U}^h, \overline{\sigma}_{ij})$, which is the one related to the buckling problem. Although not explicitly shown in the results section, the buckling eigenvalues and eigenvectors obtained from Eq.(33) were not influenced by the choice of μ when this was selected following the same recommendations specified for linear static analysis.

C. Implicitly-defined mesh

The Interior Penalty DG formulations given in Eqs.(29) and (32) for the static and the buckling problems of multilayered shells are valid regardless of the chosen meshing strategy. In fact, they may be employed in combination with conventional (e.g. triangular or structured) meshes as well as with non-conventional (e.g. polygonal) meshes.

Table 1 Properties of the considered materials.

Material ID	Property	Component	Value
M_1	Young's moduli	E_1/E_r	variable
		E_2/E_r, E_3/E_r	1
	Poisson's ratios	ν_{23}, ν_{13}, ν_{12}	0.25
	Shear moduli	G_{23}/E_r	0.5
		G_{13}/E_r, G_{12}/E_r	0.6
M_2	Young's moduli	E_1/E_r	40
		E_2/E_r, E_3/E_r	1
	Poisson's ratios	ν_{23}, ν_{13}, ν_{12}	0.25
	Shear moduli	G_{23}/E_r	0.6
		G_{13}/E_r, G_{12}/E_r	0.5

In this work, we employ the implicitly-defined mesh technique firstly introduced by Saye [60] in the context of DG methods for fluid dynamics applications. Such a meshing strategy is based on an implicit representation of the modelling domain Ω_ξ within a background rectangle $\Pi_\xi \supseteq \Omega_\xi$ by suitably introducing a level set function $\varphi = \varphi(\xi_1, \xi_2)$ such that

$$\Omega_\xi \equiv \left\{(\xi_1, \xi_2) \in \Pi_\xi \mid \varphi(\xi_1, \xi_2) < 0\right\} \tag{34a}$$

and

$$\partial\Omega_\xi \equiv \left\{(\xi_1, \xi_2) \in \partial\Pi_\xi \mid \varphi(\xi_1, \xi_2) < 0\right\} \cup \left\{(\xi_1, \xi_2) \in \Pi_\xi \mid \varphi(\xi_1, \xi_2) = 0\right\}, \tag{34b}$$

where $\partial\Pi_\xi$ denotes the boundary of Π_ξ. A background structured grid is then generated for Π_ξ and its cells are intersected with the implicitly-defined domain Ω_ξ. This leads to a classification of the cells based on their volume fraction: *entire* cells are those falling entirely inside Ω_ξ, *empty* cells are those falling entirely outside Ω_ξ, *partial* cells are those cut by the zero contour of the level set function and having a volume fraction larger than a user-defined threshold and *small* cells are those cut by the zero contour of the level set function and having a volume fraction smaller or equal to the same threshold. Small cells are merged with their nearby entire or partial cells to avoid the ill-conditioning of the discrete system of equations due to overly small volume fractions. Finally, the elements of the implicitly-defined mesh consist of the (potentially extended) entire and partial cells. As an example, Fig.(2a) shows the classification of the cells of a 9×9 background grid generated for a shell modelling domain consisting of a square with a circular hole, while the corresponding implicitly-defined mesh is displayed in Fig.(2b), which also highlights the extended elements.

The present implicit-mesh DG formulation technique exploits the ease of generation of structured grids and offers a high-order accurate resolution of the considered problem also in proximity of the cut cells thanks to the use of high-order quadrature rules for implicitly-defined domains and boundaries [53]. The interested reader is referred to Ref.[60] for a more comprehensive description of the generation of the implicitly-defined mesh and to Refs.[42, 43] for the application of the implicit-mesh DG methods to the static analysis of plates and shells. The high-order accuracy of implicit-mesh DG methods is also discussed in Refs.[61–64] in the context of elliptic and hyperbolic partial differential equations. As a last comment on the present meshing strategy, it is clear that the implicitly-defined mesh coincides with a standard structured grid when $\varphi(\xi_1, \xi_2) < 0 \; \forall (\xi_1, \xi_2) \in \Pi_\xi$.

V. Numerical results

In this section the capabilities of the proposed buckling formulation are assessed through several numerical tests. Three composite structures are investigated, namely a laminated plate, a laminated cylindrical shell and a laminated plate with a circular cut-out, under various geometrical and material configurations. In the performed tests, the adopted ESL theories are denoted by $\mathrm{ED}_{N_1N_2N_3}$ where N_i is the order of the through-the-thickness expansion of the covariant displacement component u_{ξ_i}, see Eq.(6). The FSDT is also considered as a special case of the ED_{110} theory combined with the plane stress assumption. The engineering constants of the considered materials are listed in Tab.(1), while the lamination sequences of the considered composite structures are reported in Tab.(2). Legendre polynomials are employed as thickness functions and as basis functions for the DG formulations.

A. Laminated plate

The first investigated composite structure is a multilayered square plate with simply-supported edges as illustrated in Fig.(3) , i.e. $u_{\xi_1} = u_{\xi_3} = 0$ at $\xi_1 = (0, a)$ and $u_{\xi_2} = u_{\xi_3} = 0$ at $\xi_2 = (0, a)$. The mean surface of the plate is defined through the simple map

$$\boldsymbol{x}_0 = \begin{bmatrix} \xi_1 \\ \xi_2 \\ 0 \end{bmatrix}, \tag{35}$$

Table 2 Properties of the considered shell sections.

Shell ID	Material	Layup	Layer(s) thickness
P_1	M_1	[0/90/0]	$\tau_0 = \tau/4, \tau_{90} = \tau/2$
P_2	M_1	[0/90/0/90/0/90/0/90/0]	$\tau_0 = \tau/10, \tau_{90} = \tau/8$
C_1	M_2	[0/90/0/90/0]	$\tau/5$
C_2	M_2	[0/90/0]	$\tau_0 = \tau/5, \tau_{90} = 3\tau/5$
H_1	M_1	$[(+30/-30)_2]_s$	$\tau/8$
N_1	M_2	[0/90/90/0]	$\tau/4$

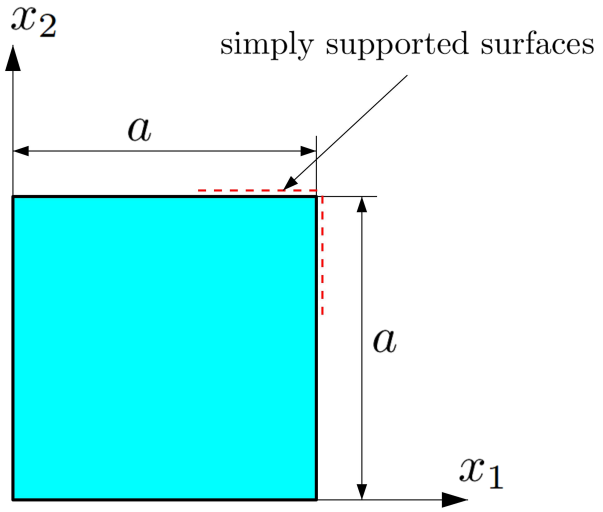

Fig. 3 Geometry of the multilayered square plate.

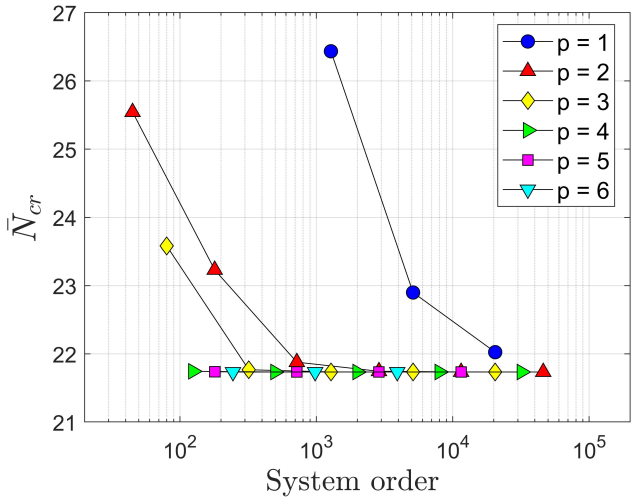

Fig. 4 Convergence of the non-dimensional buckling load for the multilayered square plate.

Table 3 Non-dimensional buckling load for multilayered plate as a function of the ESL theory, the orthotropy ratio E_1/E_r and the stacking sequence. The results obtained in [9] using a 3D model are also reported for comparison purposes. Here, the thickness ratio is $a/\tau = 10$.

	$E_1/E_r = 3$	10	20	30	40
P_1					
3D [9]	5.3044	9.7621	15.0191	19.3040	22.8807
ED_{333} [18]	5.3060	9.7720	15.0551	19.3785	23.0021
ED_{333}	5.3058	9.7713	15.0536	19.3760	22.9986
ED_{222} [18]	5.3556	9.9945	15.6458	20.4027	24.4816
ED_{222}	5.3554	9.9939	15.6441	20.3999	24.4775
$FSDT_{VK}$ [18]	5.3991	9.9653	15.3513	19.7566	23.4529
FSDT	5.2927	9.7578	15.0573	19.4104	23.0734
P_2					
3D [9]	5.3352	10.0417	15.9153	20.9614	25.3436
ED_{333} [18]	5.3385	10.0578	15.9629	21.0501	25.4786
ED_{333}	5.3383	10.0572	15.9613	21.0474	25.4746
ED_{222} [18]	5.3810	10.2301	16.4245	21.8793	26.7207
ED_{222}	5.3809	10.2294	16.4228	21.8763	26.7164
$FSDT_{VK}$ [18]	5.4126	10.1895	16.1459	21.2650	25.7152
FSDT	5.3261	10.0341	15.9295	21.0141	25.4462

where $(\xi_1, \xi_2) \in \Omega_\xi \equiv [0, a] \times [0, a]$. A uniform initial stress state is assumed for each layer and is defined by setting

$$\overline{\sigma}_{11}^{\langle \ell \rangle} = -c_{11}^{\langle \ell \rangle} \varepsilon^0, \quad \text{and} \quad \overline{\sigma}_{22}^{\langle \ell \rangle} = -\chi c_{22}^{\langle \ell \rangle} \varepsilon^0 \tag{36}$$

and all other components to zero. In Eq.(36) ε^0 is a reference strain, $c_{11}^{\langle \ell \rangle}$ and $c_{22}^{\langle \ell \rangle}$ are elements of the stiffness matrix of the ℓ-th layer and χ is a parameter that is equal to 0 for uniaxial compression and 1 for biaxial compression. The non-dimensional critical buckling load is defined as follows

$$\overline{N}_{cr} \equiv \lambda \frac{a^2}{E_r \tau^3} \sum_{\ell=1}^{N_\ell} \int_{\xi_{3b}^{\langle \ell \rangle}}^{\xi_{3t}^{\langle \ell \rangle}} \overline{\sigma}_{11}^{\langle \ell \rangle} \mathrm{d}\xi_3, \tag{37}$$

where λ is the smallest eigenvalue obtained by solving the problem in Eq.(32).

We initially consider the stacking sequence denoted by P_1 in Tab.(2) with thickness ratio $a/\tau = 20$, orthotropy ratio $E_1/E_r = 25$ and $\chi = 0$, and partition the modelling domain of the plate using a simple structured grid consisting of $N_e = n_e^2$ elements, being n_e the number of elements per side of the modelling domain. The plate is modelled using the FSDT. The value of the non-dimensional critical buckling load $\overline{N}_{cr}$ given in Eq.(37) is then computed as a function of the degree p of the basis functions and the number of elements N_e. Figure (4) reports the obtained values of $\overline{N}_{cr}$ as a function of the system order defined as $N_e N_p N_U$ where $N_p \equiv (1 + p)^2$. As depicted in the figure, higher-order DG formulations show a faster convergence of the critical buckling load and use a smaller number of degrees of freedom to obtain the converged result with respect to lower-order formulations.

The value of $\overline{N}_{cr}$ is then computed using a 4×4 grid and $p = 6$ polynomial basis functions, and the effect of thickness ratio a/τ, the orthotropy ratio E_1/E_r, the biaxial load parameter χ and the selected shell theory is investigated. Table (3) reports the values of $\overline{N}_{cr}$ as a function of the ESL theory and the ratio E_1/E_r for the stacking sequences denoted by P_1 and P_2 in Tab.(2) with thickness ratio $a/\tau = 10$. The effect of the biaxial load parameter χ on the critical buckling load is reported in Tab.(4) for five different values of the thickness ratio a/τ and for two ESL theories upon selecting an orthotropy ratio equal to $E_1/E_r = 25$ and the stacking sequence P_1. In both Tab.(3) and (4), the results obtained with the present formulation are compared with those obtained in [9] via a 3D model and those obtained in [18] using different ESL theories. In all cases, an excellent agreement between the present DG formulation and the reference models is observed. The largest differences might be noticed in the results obtained using the FSDT and are due the adoption of the Von Karman hypotheses in the referenced work. It is however worth noting that using the full set of non-linear strain components also for the FSDT provides more accurate results if compared with the 3D solution.

Table 4 Non-dimensional uniaxial and biaxial buckling load as a function of two shell theories and different thickness ratios a/τ. Here, the orthotropy ratio is $E_1/E_r = 25$ and the stacking sequence is P_1.

	$a/\tau = 10$	20	25	50	100
$\chi = 0$					
ED_{444} [18]	17.3127	21.7304	22.4358	23.4593	23.7316
ED_{444}	17.3106	21.7300	22.4356	23.4593	23.7316
$FSDT_{VK}$ [18]	17.6568	21.8687	22.5307	23.4855	23.7383
FSDT	17.3336	21.7344	22.4382	23.4599	23.7317
$\chi = 1$					
ED_{444} [18]	8.7057	10.8849	11.2314	11.7334	11.8668
ED_{444}	8.7052	10.8848	11.2314	11.7334	11.8668
$FSDT_{VK}$ [18]	8.8284	10.9344	11.2654	11.7428	11.8692
FSDT	8.7324	10.8946	11.2380	11.7352	11.8672

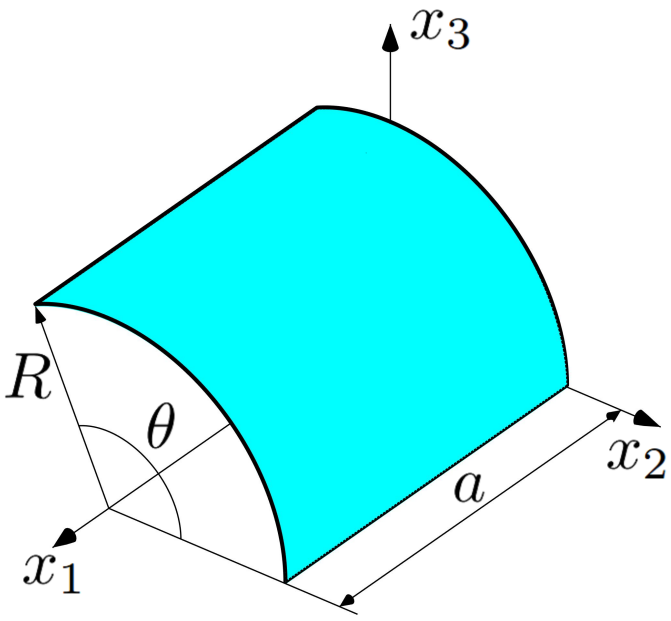

Fig. 5 Geometry of the multilayered cylindrical shell.

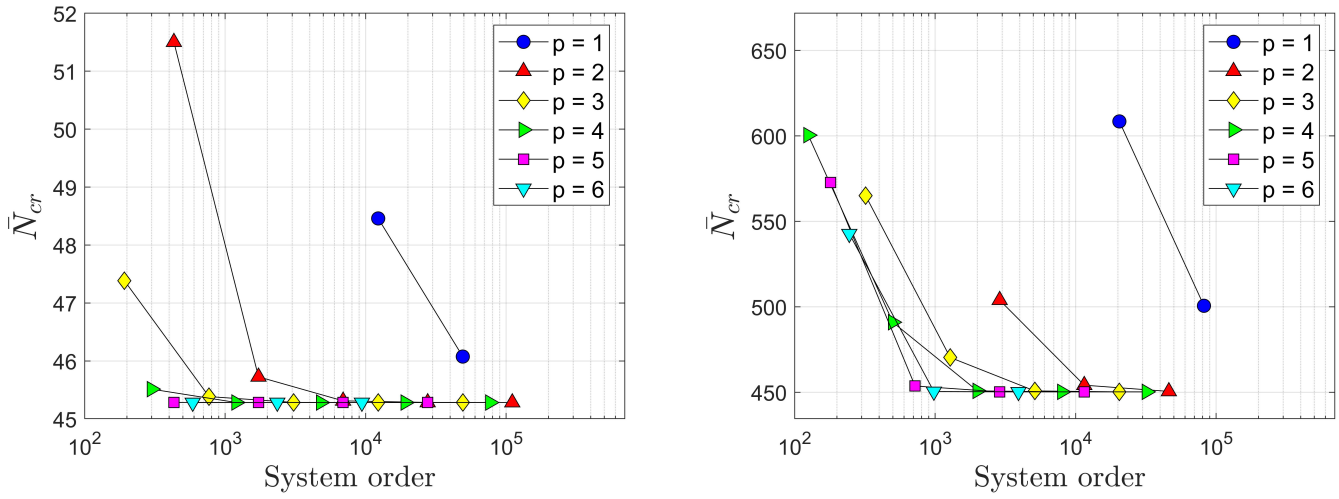

(a) **(b)**

Fig. 6 Convergence of the non-dimensional buckling load for the multilayered cylindrical shell C_1 with (a) $a/\tau = 20$ and $a/R = 1$ and (b) $a/\tau = 100$ and $a/R = 2$.

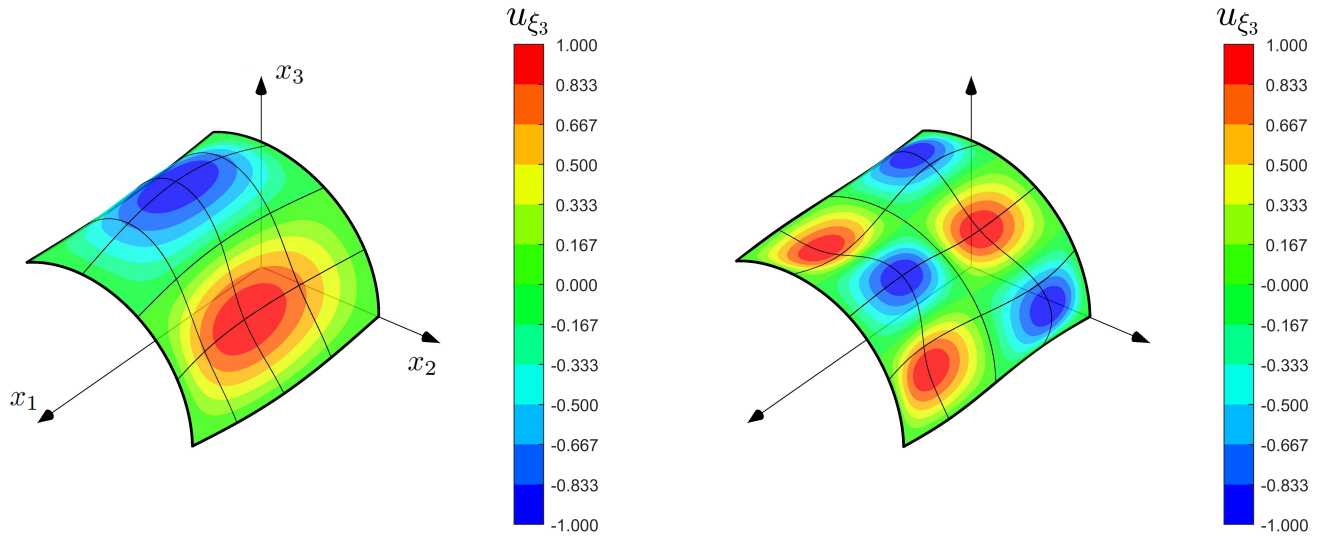

(a) **(b)**

Fig. 7 Sample buckling mode for the cylindrical shell C_1 with (a) $a/\tau = 50$ and $a/R = 2$ and (b) $a/\tau = 100$ and $a/R = 2$.

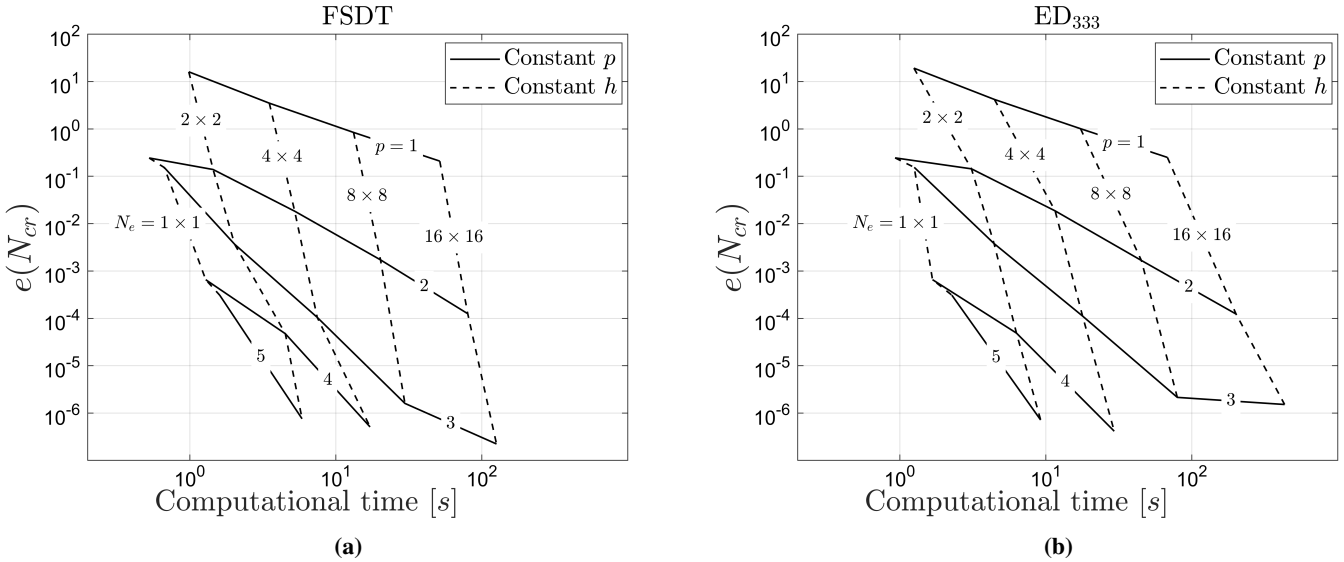

(a) **(b)**

Fig. 8 Error in the first buckling load of the cylindrical shell C_1 with $a/R = 0.05$ and $a/\tau = 50$ as function of the computational time for different values of the polynomial order and the number of mesh elements. (a) FSDT and (b) ED_{333} theory. Computational time of the analysis for different numbers of elements and orders of the polynomials.

B. Laminated cylindrical shell

The second set of tests are referred to the cylindrical shell shown in Fig.(5). The shell mean surface is defined as

$$\boldsymbol{x}_0 = \begin{bmatrix} \xi_1 \\ R\cos(\xi_2) \\ R\sin(\xi_2) \end{bmatrix}, \tag{38}$$

where $(\xi_1, \xi_2) \in \Omega_\xi \equiv [0, a] \times [0, \theta]$ and $\theta = a/R$. The shell is simply-supported and subjected to a uniform initial stress state defined by setting

$$\overline{\sigma}_{11}^{\langle \ell \rangle} = -\sigma^0 \tag{39}$$

and zero in all other components. In this case, the following non-dimensional critical buckling load is employed

$$\overline{N}_{cr} \equiv \lambda \frac{\sigma^0 a^2}{E_r \tau^2}. \tag{40}$$

The stacking sequence denoted by C_1 in Tab.(2) is considered for this set of tests. We perform a similar convergence analysis to the one presented in Sec.(V.A) for a cylindrical shell characterized by $a/\tau = 20$ and $a/R = 1$ and modelled using the ED_{333} theory and a cylindrical shell characterized by $a/\tau = 100$ and $a/R = 2$ and modelled using the FSDT theory. Figure (6) reports the computed value of the critical buckling load given in Eq.(40) as a function of the system order and, similarly to what observed in Fig.(4), shows the benefit of using higher-order methods in terms of convergence rate and overall number of degrees of freedom.

The value of $\overline{N}_{cr}$ is then computed using a 4×4 grid and $p = 6$ polynomial basis functions for different ESL theories and different values of the ratios a/τ and a/R. Table (5) reports the computed values of $\overline{N}_{cr}$ as a function of various ESL theories and the ratio a/τ for the cylindrical shell with $a/R = 0.05$. A similar parametric analysis is reported in Tab.(6), where we consider the FSDT and the ED_{444} theory and change the ratios a/τ and a/R. Similarly to the plate case, Tab.(5) and (6) also report the reference critical buckling load $\overline{N}_{cr}$ obtained in [18], and confirm the accuracy of the present formulation. As an example, the first buckling mode of the cylindrical shell characterized by $a/R = 2$ and $a/\tau = 50$ and the cylindrical shell characterized by $a/R = 2$ and $a/\tau = 100$, both modelled by the FSDT theory, are displayed in Fig.(7). By looking at Fig.(6), it is possible to notice that using high-order polynomials allows achieving convergence of the buckling load with a smaller number of overall degrees of freedom with respect to using low-order polynomials. This is valid for both buckling eigenmodes that involve a small number and a large number of half waves throughout the structure. Eventually, to further illustrate the advantages of using high-order approximations, the error in first buckling load for the shell C_1 with $a/R = 0.05$ and $a/\tau = 50$ is plotted as a function of the computational time for different values of order p of the polynomial basis functions and of number N_e of mesh elements. The obtained results are reported in Figs.(8a) and (8b) for the FSDT and the ED_{333} theory, respectively, and clearly show the superior performance of higher-order basis functions with respect to low-order basis functions in terms of computational time required to achieve a given level of accuracy. In other words, the results obtained for the considered numerical tests suggest that using higher-order polynomial basis functions in combination with a coarser mesh is preferable over low-order polynomials combined with a finer mesh, regardless of the chosen through-the-thickness expansion.

Table 5 Non-dimensional buckling load for the multilayered cylindrical shell C_1 as a function of the shell theory and the thickness ratio a/τ. Here, $a/R = 0.05$.

	$a/\tau = 10$	20	30	50	100
ED_{444} [18]	24.20	31.94	34.06	35.42	36.85
ED_{444}	24.19	31.94	34.06	35.42	36.85
ED_{333} [18]	24.20	31.94	34.06	35.42	36.85
ED_{333}	24.19	31.94	34.06	35.42	36.85
ED_{222} [18]	25.27	32.37	34.27	35.50	36.87
ED_{222}	25.26	32.37	34.27	35.50	36.87
$FSDT_{VK}$ [18]	24.18	31.90	34.04	35.42	36.85
FSDT	23.95	31.78	33.97	35.39	36.84

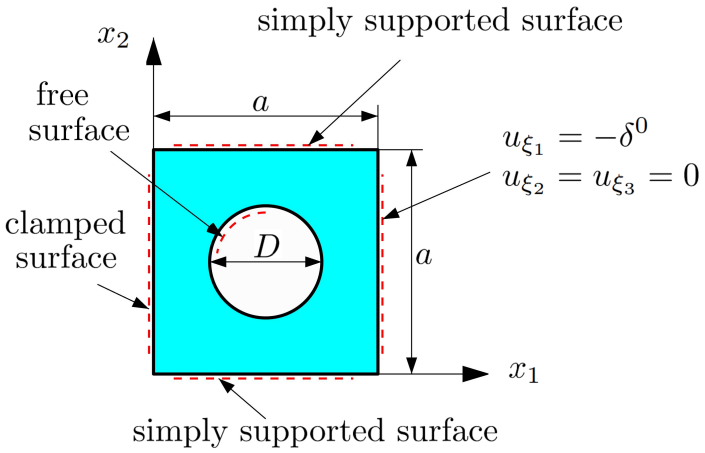

Fig. 9 Geometry of the multilayered square plate with a circular cut-out.

As the last test on cylindrical shell structures, the advantage of employing higher-order through-the-thickness approximations is investigated. The cylindrical shell C_2 with $a/R = 0.5$ and variable a/τ is considered. The shell is clamped at the surface corresponding to $\xi_1 = 0$, a pressure $\bar{t}_1 = -q^0$ is applied on the surface corresponding to $\xi_1 = a$, while the other edges are kept free. In this test, the initial stress field $\overline{\sigma}_{ij}^{\langle \ell \rangle}$ is computed as a result of the corresponding linear static analysis. The tests are carried out with a 2×2 structured grid and a polynomial order $p = 6$. For these analyses, the non-dimensional critical buckling load is computed as

$$\overline{N}_{cr} \equiv \lambda \frac{q^0 a^2}{E_r \tau^2}. \tag{41}$$

Table (7) reports the computed values of the buckling load for three different ratios a/τ and different shell theories, namely the FSDT, the ED_{333} and the ED_{444} theories. The table also reports the buckling loads computed with a three-dimensional analysis using the C3D20R elements implemented in Abaqus [65]. The obtained results show that the buckling load computed with the FSDT matches the three-dimensional result when the shell is relatively thin but differs noticeably for larger values of the thickness. In the latter case, high-order through-the-thickness expansions recover the three-dimensional solutions and their use is recommended.

C. Laminated Plate with circular cut-out

In the third set of tests, the critical buckling load is computed for the laminated plate with a circular cut-out shown in Fig.(9). For these tests, the implicit-mesh DG formulation is employed. The shell mean surface is described by the map given in Eq.(35) with $(\xi_1, \xi_2) \in \Omega_\xi \equiv [0, a] \times [0, a]$. The mesh of the domain is constructed starting from a 15×15 background grid, while the space of basis functions uses $p = 3$ polynomials. The modelling domain of the plate is implicitly-defined via the following level-set function

$$\phi(\xi_1, \xi_2) = \frac{D^2}{4} - \left(\xi_1 - \frac{a}{2}\right)^2 - \left(\xi_2 - \frac{a}{2}\right)^2, \tag{42}$$

where D is the diameter of the circular cut-out. The stacking sequence denoted by H_1 in Tab.(2) is considered for these tests.

Unlike the two previous sets of tests, where the initial stress was prescribed as a constant field, the initial stress distribution for this test case is computed from a linear elastic static analysis. The boundary condition of the static analysis are as follows: the boundaries at $\xi_2 = 0$ and $\xi_2 = a$ are simply supported, i.e. $u_{\xi_2} = u_{\xi_3} = 0$; the boundary at $\xi_1 = 0$ is clamped; and the boundary at $\xi_1 = a$ is subjected to

Table 6 Non-dimensional buckling load for the multilayered cylindrical shell C_1 as a function of two shell theories and the ratios a/τ and a/R.

	$a/\tau = 10$	20	50	100
$a/R = 0.1$				
ED_{444} [18]	24.20	32.05	36.29	40.42
ED_{444}	24.20	32.05	36.29	40.42
$FSDT_{VK}$ [18]	24.21	32.04	36.31	40.46
FSDT [18]	23.97	31.90	36.25	40.41
FSDT	23.96	31.90	36.26	40.42
$a/R = 0.2$				
ED_{444} [18]	24.23	32.49	39.74	54.67
ED_{444}	24.24	32.49	39.74	54.67
$FSDT_{VK}$ [18]	24.31	32.57	39.88	54.88
FSDT [18]	24.00	32.33	39.70	54.67
FSDT	24.00	32.34	39.71	54.67
$a/R = 1$				
ED_{444} [18]	25.26	45.28	140.6	253.3
ED_{444}	25.26	45.28	140.6	253.3
$FSDT_{VK}$ [18]	27.63	49.61	154.1	259.4
FSDT [18]	25.03	45.14	140.6	253.2
FSDT	25.11	45.26	140.7	253.4
$a/R = 2$				
ED_{444} [18]	28.23	74.97	220.1	448.2
ED_{444}	28.23	74.97	220.2	448.2
$FSDT_{VK}$ [18]	38.90	103.9	243.7	469.1
FSDT [18]	27.96	74.84	221.3	448.9
FSDT	28.08	75.02	223.1	450.2

Table 7 Non-dimensional buckling load for the multilayered cylindrical shell C_2 as a function of the shell theories and the ratio a/τ for $a/R = 0.5$.

	$a/\tau = 20$	10	5
FSDT	3.971	2.350	1.752
ED_{333}	3.957	2.310	1.634
ED_{444}	3.956	2.308	1.631
C3D20R elements [65]	3.965	2.309	1.631

Table 8 Non-dimensional displacement at buckling for the multilayered plate with the circular cut-out H_1 as a function of different shell theories and the ratios a/τ and D/a.

	$a/\tau = 20$	50	100
$D/a = 0$			
S4R elements [65]	3.231	4.093	4.268
FSDT	3.229	4.080	4.253
ED_{222}	3.367	4.119	4.265
ED_{333}	3.215	4.078	4.253
ED_{444}	3.216	4.078	4.253
$D/a = 0.1$			
S4R elements [65]	3.216	4.035	4.207
FSDT	3.217	4.035	4.208
ED_{222}	3.350	4.074	4.221
ED_{333}	3.203	4.032	4.208
ED_{444}	3.204	4.033	4.209
$D/a = 0.25$			
S4R elements [65]	3.770	4.716	4.914
FSDT	3.759	4.709	4.908
ED_{222}	3.922	4.758	4.924
ED_{333}	3.745	4.709	4.910
ED_{444}	3.747	4.710	4.911
$D/a = 0.5$			
S4R elements [65]	5.670	7.858	8.418
FSDT	5.626	7.850	8.427
ED_{222}	5.977	7.986	8.481
ED_{333}	5.576	7.848	8.435
ED_{444}	5.581	7.850	8.436
$D/a = 0.75$			
S4R elements [65]	9.836	17.318	19.748
FSDT	9.732	17.252	19.734
ED_{222}	10.714	17.783	19.954
ED_{333}	9.493	17.127	19.709
ED_{444}	9.501	17.133	19.713

a uniform displacement given by $u_{\xi_1} = -\delta^0$ and $u_{\xi_2} = u_{\xi_3} = 0$. The non-dimensional critical value of the applied displacement for which the buckling occurs is computed as

$$\overline{u}_{cr} \equiv \lambda \frac{\delta^0 a}{\tau^2}. \tag{43}$$

Tab.(8) reports the computed values of $\overline{u}_{cr}$ as a function of the selected ESL theory, the hole diameter D and the thickness ratio a/τ for the stacking sequence denoted by H_1 in Tab.(2). The obtained results and are compared with those obtained with Abaqus using the S4R elements and demonstrate the accuracy of the present DG formulation combined with the implicitly-defined mesh technique. The first buckling mode for the plate characterized by $a/\tau = 50$ and $D/a = 0.5$ and modelled with the FSDT theory is displayed in Fig.(10).

D. Laminated generally-curved NURBS-based shell

In the final set of tests, the present formulation is employed to perform the buckling analysis of a generally-curved shell with and without a cut-out. The shell mean surface is described by a NURBS parametrization [66, 67] whose control points, weights, order and knot vectors are provided in details in [42]. The shell also contains a cut-out that is implicitly defined by the following level set function

$$\phi(\boldsymbol{x}_0) = a^d - |x_{01} - x_{1n}|^d - |x_{02} - x_{2n}|^d \,. \tag{44}$$

The geometrical parameters appearing in Eq.(44) and in Fig.(11), which shows the shell geometry from three different views, are given in Tab.(9). It is worth noting that the level set function of the variables x_{01} and x_{02} is easily transformed into a function of the curvilinear

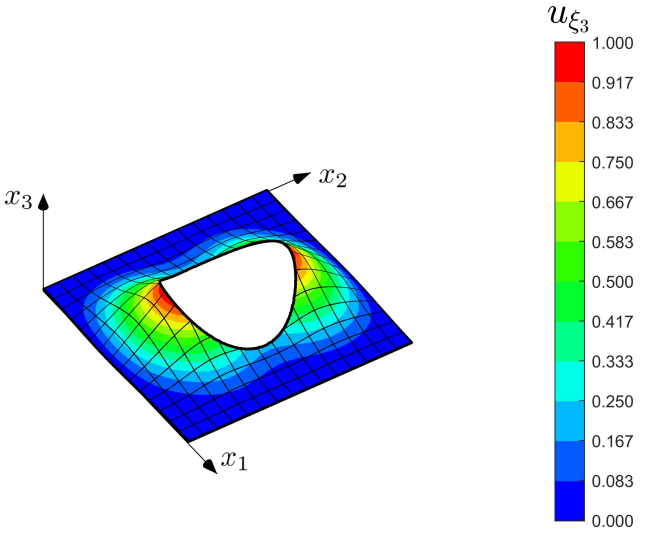

Fig. 10 Sample buckling mode for the laminated plate with cut-out.

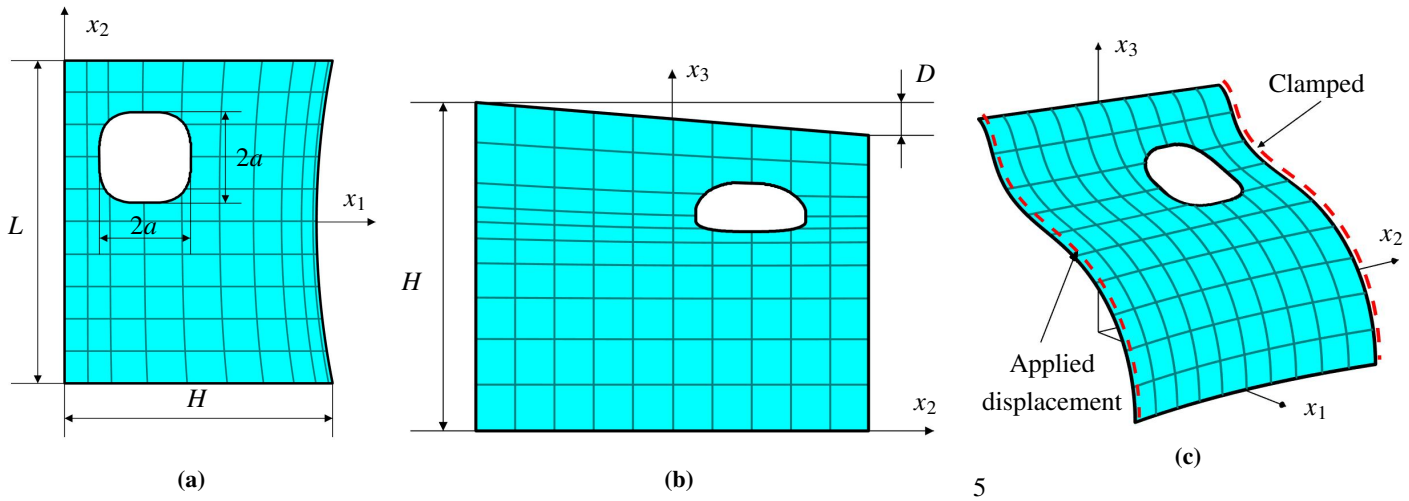

5

Fig. 11 Geometry of the generally-curved NURBS-based shell in three different views with superimposed mesh boundaries.

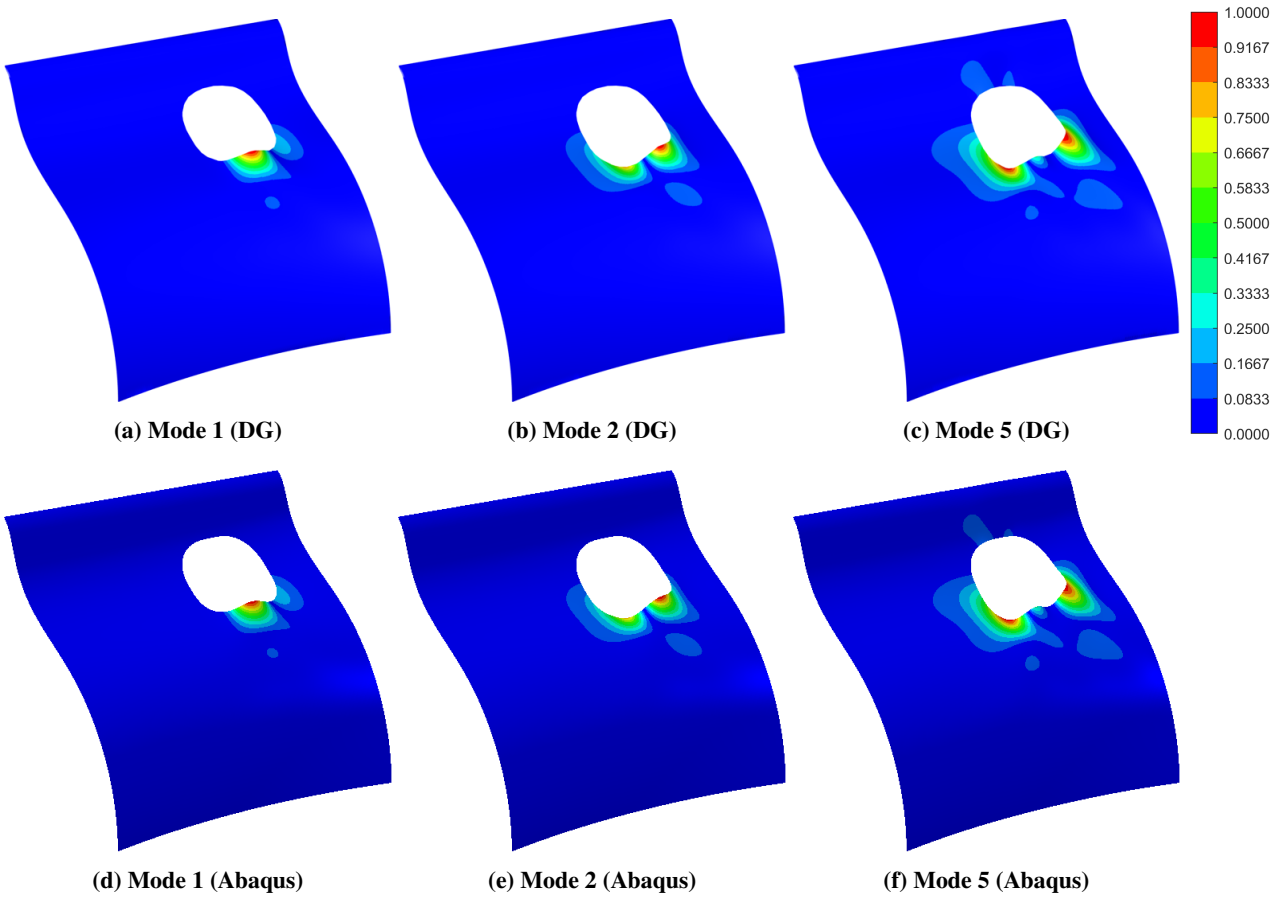

(a) Mode 1 (DG) **(b) Mode 2 (DG)** **(c) Mode 5 (DG)**

(d) Mode 1 (Abaqus) **(e) Mode 2 (Abaqus)** **(f) Mode 5 (Abaqus)**

Fig. 12 Buckling modes for the NURBS-based shell N_1 with the cut-out in terms of the magnitude of the displacement.

variables ξ_1 and ξ_2 by using the the map of the mean surface introduced in Eq.(1).

As sketched in Fig.(11c), the shell is clamped at the surface corresponding to $\xi_2 = 1$, while a uniform displacement $\overline{\boldsymbol{u}} = (0, \delta^0, 0)$ is applied at the surface $\xi_2 = 0$; the other boundaries are kept free. The considered shell section is the one denoted by N_1 in Tab.(2), while the selected shell theory is the FSDT. The eigenvalue problem is solved by the present DG formulation using 10×10 grid and a polynomial order $p = 6$. The same problem is solved by the FEM software library Abaqus using S3 elements and S4R elements for the shell with the cut-out and without the cut-out, respectively. The comparison between the obtained results is given in Tab.(10) in terms of the 1st, 2nd and 5th values of the following non-dimensional critical loading

$$\overline{u}_{cr} \equiv \lambda \frac{\delta^0 H}{\tau^2}. \tag{45}$$

An excellent agreement is observed for all values of the critical loading for the shell with and without the cut-out. Eventually, the comparison between the eigenmodes obtained with the present formulation and with Abaqus and corresponding to the 1st, 2nd and 5th eigenvalues is reported in Fig.(12) for the shell with the cut-out and in Fig.(13) for the shell without the cut-out. An excellent matching is also observed for the eigenmodes of the problem.

As a last comment, it is worth mentioning that, for a structure where there is coupling between membrane and flexural behaviour, the physical meaning of a linear buckling analysis is questionable as a clear bifurcation in the loading path is not present. However, the results obtained by the linear buckling analysis provide useful information regarding the structure response in the finite-deformation regime, indicating when the stiffness may undergo a significant decrease. A DG formulation for a fully non-linear analysis of multilayered shells is currently under investigation and will be presented in future studies.

VI. Conclusions

In this work, a novel formulation for the linear buckling analysis of multilayered plates and shells was presented. The formulation is based on the use of ESL theories to model the mechanical behavior of multilayered structures and on the use of implicit-mesh Interior Penalty DG methods for solving the linear buckling problem.

Starting from the three-dimensional variational statement of Eulerian buckling and introducing the through-the-thickness expansion of the covariant components of the displacement field, the variational statement of Eulerian buckling for laminated structures modelled by ESL theories was derived in terms of generalized displacement variables. Then, the variational statement was employed to formulate the

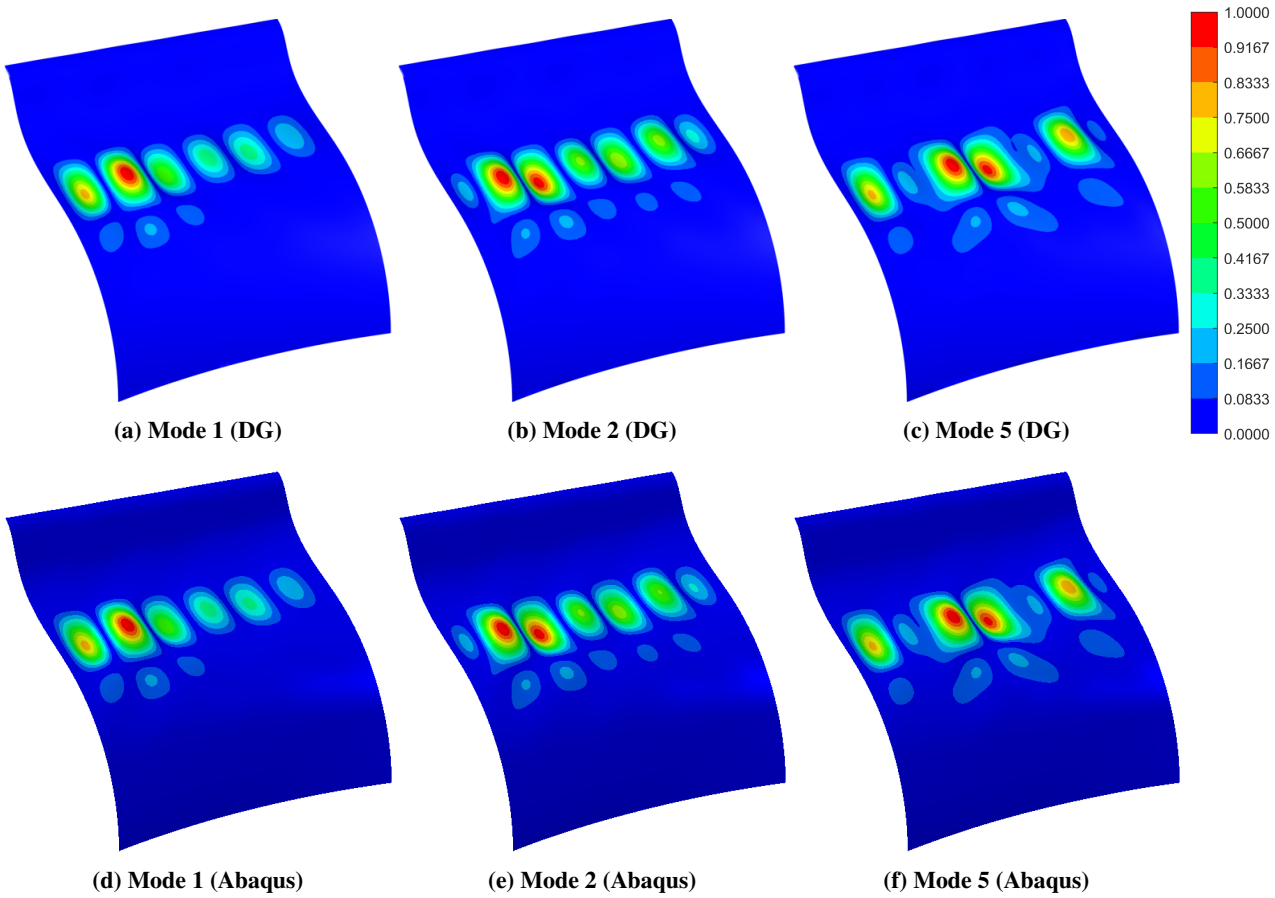

(a) Mode 1 (DG) **(b) Mode 2 (DG)** **(c) Mode 5 (DG)**

(d) Mode 1 (Abaqus) **(e) Mode 2 (Abaqus)** **(f) Mode 5 (Abaqus)**

Fig. 13 Buckling modes for the NURBS-based shell N_1 without the cut-out in terms of the magnitude of the displacement.

proposed Interior Penalty DG scheme, which is based on a discontinuous representation of the approximated solution throughout the mesh elements and on the use of suitably defined boundary integrals to enforce the inter-element solution continuity and the boundary conditions. To account for the presence of cutouts, the DG scheme was implemented in conjunction with the implicitly-defined mesh technique, whereby the shell modelling domain is implicitly represented via a level set function and the mesh elements are constructed by intersecting an easy-to-generate background grid and the implicitly-defined domain.

The capabilities of the proposed formulation were assessed through various numerical tests conducted on multilayered shells modelled by different ESL theories, including the FSDT as a special case, and characterized by different stacking sequences and boundary conditions. Three geometries were investigated: a square plate, a cylindrical shell and a square plate with a central circular cutout. Convergence analyses were performed on the critical buckling load for the square plate and the cylindrical shell subjected to a prescribed stress distribution. The computed values of the buckling load was reported as a function of the number of mesh elements and degree of the polynomial basis functions. The obtained results confirmed the benefit of using higher-order DG methods to achieve faster convergence rates with a smaller number of degrees of freedom with respect to lower-order DG methods. The buckling analysis on the square plate with the circular cutout was performed using the initial stress distribution obtained from a static analysis. For all the numerical tests,

Table 9 Geometrical parameters for the NURBS-based generally-curved shell.

NURBS-based shell	
H	50 cm
D	5 cm
L	60 cm
a	8.5 cm
d	3
x_{1n}	15 cm
x_{2n}	12 cm
τ	1 mm

Table 10 Non-dimensional displacement at buckling for the NURBS-based shell N_1 with and without the cut-out.

Shell geometry	1st (DG)	1st (FEM)	2nd (DG)	2nd (FEM)	5th (DG)	5th (FEM)
With cut-out	34.31	34.38	36.02	36.12	58.47	58.51
Without cut-out	61.75	62.09	62.42	62.77	70.35	70.76

the obtained values of the critical buckling load were compared with reference results taken from the existing literature or with those computed using the standard FEM software library Abaqus [65]. Excellent agreement between the proposed formulation and the reference models was always observed.

In the future, the present approach for the study of laminated structures will be extended to account for free and forced vibration problems, finite deformation elasticity and the analysis of plate and shell assemblies, which are currently under investigation.

References

[1] Crisfield, M., "An arc-length method including line searches and accelerations," *International journal for numerical methods in engineering*, Vol. 19, No. 9, 1983, pp. 1269–1289. https://doi.org/10.1002/nme.1620190902.

[2] Chia, C.-Y., "Geometrically Nonlinear Behavior of Composite Plates: A Review," *Applied Mechanics Reviews*, Vol. 41, No. 12, 1988, pp. 439–451. https://doi.org/10.1115/1.3151873.

[3] Noor, A. K., and Peters, J. M., "Buckling and postbuckling analyses of laminated anisotropic structures," *International Journal for Numerical Methods in Engineering*, Vol. 27, No. 2, 1989, pp. 383–401. https://doi.org/10.1002/nme.1620270211.

[4] Turvey, G. J., and Marshall, I. H., *Buckling and postbuckling of composite plates*, Springer Science & Business Media, 1994.

[5] Shen, H.-S., *Postbuckling behavior of plates and shells*, World Scientific, 2017.

[6] Washizu, K., *Variational Methods in Elasticity and Plasticity*, Pergamon, 1975.

[7] Donnell, L. H., "A new theory for the buckling of thin cylinders under axial compression and bending," *Trans. Am. Soc. Mech. Eng*, Vol. 56, 1934, pp. 795–806.

[8] Jones, R. M., "Buckling and vibration of unsymmetrically laminated cross-ply rectangular plates," *AIAA journal*, Vol. 11, No. 12, 1973, pp. 1626–1632. https://doi.org/10.2514/3.50660.

[9] Noor, A. K., "Stability of multilayered composite plates," *Fibre Science and Technology*, Vol. 8, No. 2, 1975, pp. 81–89. https://doi.org/10.1016/0015-0568(75)90005-6.

[10] Carrera, E., "The effects of shear deformation and curvature on buckling and vibrations of cross-ply laminated composite shells," *Journal of Sound and Vibration*, Vol. 150, No. 3, 1991, pp. 405–433. https://doi.org/10.1016/0022-460X(91)90895-Q.

[11] Reddy, J., and Khdeir, A., "Buckling and vibration of laminated composite plates using various plate theories," *AIAA journal*, Vol. 27, No. 12, 1989, pp. 1808–1817. https://doi.org/10.2514/3.10338.

[12] Khdeir, A., and Librescu, L., "Analysis of symmetric cross-ply laminated elastic plates using a higher-order theory: Part II—Buckling and free vibration," *Composite Structures*, Vol. 9, No. 4, 1988, pp. 259–277. https://doi.org/10.1016/0263-8223(88)90048-7.

[13] Nosier, A., and Reddy, J., "On vibration and buckling of symmetric laminated plates according to shear deformation theories," *Acta mechanica*, Vol. 94, No. 3, 1992, pp. 123–144. https://doi.org/10.1007/BF01176647.

[14] Reddy, J., and Starnes Jr, J., "General buckling of stiffened circular cylindrical shells according to a layerwise theory," *Computers & Structures*, Vol. 49, No. 4, 1993, pp. 605–616. https://doi.org/10.1016/0045-7949(93)90065-L.

[15] Xavier, P. B., Chew, C., and Lee, K., "Buckling and vibration of multilayer orthotropic composite shells using a simple higher-order layerwise theory," *International journal of solids and structures*, Vol. 32, No. 23, 1995, pp. 3479–3497. https://doi.org/10.1016/0020-7683(95)00002-R.

[16] D'Ottavio, M., "A Sublaminate Generalized Unified Formulation for the analysis of composite structures," *Composite Structures*, Vol. 142, 2016, pp. 187–199. https://doi.org/10.1016/j.compstruct.2016.01.087.

[17] Carrera, E., "Theories and finite elements for multilayered plates and shells: a unified compact formulation with numerical assessment and benchmarking," *Archives of Computational Methods in Engineering*, Vol. 10, No. 3, 2003, pp. 215–296. https://doi.org/10.1007/BF02736224.

[18] D'Ottavio, M., and Carrera, E., "Variable-kinematics approach for linearized buckling analysis of laminated plates and shells," *AIAA journal*, Vol. 48, No. 9, 2010, pp. 1987–1996. https://doi.org/10.2514/1.J050203.

[19] Carrera, E., Azzara, R., Daneshkhah, E., Pagani, A., and Wu, B., "Buckling and post-buckling of anisotropic flat panels subjected to axial and shear in-plane loadings accounting for classical and refined structural and nonlinear theories," *International Journal of Non-Linear Mechanics*, Vol. 133, 2021, p. 103716. https://doi.org/10.1016/j.ijnonlinmec.2021.103716.

[20] Farrokh, M., Afzali, M., and Carrera, E., "Mechanical and thermal buckling loads of rectangular FG plates by using higher-order unified formulation," *Mechanics of Advanced Materials and Structures*, Vol. 28, No. 6, 2021, pp. 608–617. https://doi.org/10.1080/15376494.2019.1578014.

[21] Thai, C. H., Nguyen-Xuan, H., Nguyen-Thanh, N., Le, T.-H., Nguyen-Thoi, T., and Rabczuk, T., "Static, free vibration, and buckling analysis of laminated composite Reissner–Mindlin plates using NURBS-based isogeometric approach," *International Journal for Numerical Methods in Engineering*, Vol. 91, No. 6, 2012, pp. 571–603. https://doi.org/10.1002/nme.4282.

[22] Alesadi, A., Galehdari, M., and Shojaee, S., "Free vibration and buckling analysis of cross-ply laminated composite plates using Carrera's unified formulation based on Isogeometric approach," *Computers & Structures*, Vol. 183, 2017, pp. 38–47. https://doi.org/10.1016/j.compstruc.2017.01.013.

[23] Alesadi, A., Galehdari, M., and Shojaee, S., "Free vibration and buckling analysis of composite laminated plates using layerwise models based on isogeometric approach and Carrera unified formulation," *Mechanics of Advanced Materials and Structures*, Vol. 25, No. 12, 2018, pp. 1018–1032. https://doi.org/10.1080/15376494.2017.1342883.

[24] Guo, Y., Do, H., and Ruess, M., "Isogeometric stability analysis of thin shells: From simple geometries to engineering models," *International Journal for Numerical Methods in Engineering*, Vol. 118, No. 8, 2019, pp. 433–458. https://doi.org/10.1002/nme.6020.

[25] Faroughi, S., Shafei, E., and Rabczuk, T., "Anisotropic solid-like shells modeled with NURBS-based isogeometric approach: vibration, buckling, and divergence analyses," *Computer Methods in Applied Mechanics and Engineering*, Vol. 359, 2020, p. 112668. https://doi.org/10.1016/j.cma.2019.112668.

[26] Nasirmanesh, A., and Mohammadi, S., "XFEM buckling analysis of cracked composite plates," *Composite Structures*, Vol. 131, 2015, pp. 333–343. https://doi.org/10.1016/j.compstruct.2015.05.013.

[27] Nasirmanesh, A., and Mohammadi, S., "Eigenvalue buckling analysis of cracked functionally graded cylindrical shells in the framework of the extended finite element method," *Composite Structures*, Vol. 159, 2017, pp. 548–566. https://doi.org/10.1016/j.compstruct.2016.09.065.

[28] Milazzo, A., Benedetti, I., and Gulizzi, V., "An extended Ritz formulation for buckling and post-buckling analysis of cracked multilayered plates," *Composite Structures*, Vol. 201, 2018, pp. 980–994. https://doi.org/10.1016/j.compstruct.2018.06.026.

[29] Milazzo, A., Benedetti, I., and Gulizzi, V., "A single-domain Ritz approach for buckling and post-buckling analysis of cracked plates," *International Journal of Solids and Structures*, Vol. 159, 2019, pp. 221–231. https://doi.org/10.1016/j.ijsolstr.2018.10.002.

[30] Gulizzi, V., Oliveri, V., and Milazzo, A., "Buckling and post-buckling analysis of cracked stiffened panels via an X-Ritz method," *Aerospace Science and Technology*, Vol. 86, 2019, pp. 268–282. https://doi.org/10.1016/j.ast.2019.01.019.

[31] Sciascia, G., Oliveri, V., and Weaver, P. M., "Eigenfrequencies of prestressed variable stiffness composite shells," *Composite Structures*, Vol. 270, 2021, p. 114019. https://doi.org/10.1016/j.compstruct.2021.114019.

[32] Sciascia, G., Oliveri, V., and Weaver, P. M., "Dynamic analysis of prestressed variable stiffness composite shell structures," *Thin-Walled Structures*, Vol. 175, 2022, p. 109193. https://doi.org/10.1016/j.tws.2022.109193.

[33] Vescovini, R., and Dozio, L., "A variable-kinematic model for variable stiffness plates: Vibration and buckling analysis," *Composite Structures*, Vol. 142, 2016, pp. 15–26. https://doi.org/10.1016/j.compstruct.2016.01.068.

[34] Vescovini, R., Dozio, L., D'Ottavio, M., and Polit, O., "On the application of the Ritz method to free vibration and buckling analysis of highly anisotropic plates," *Composite Structures*, Vol. 192, 2018, pp. 460–474. https://doi.org/10.1016/j.compstruct.2018.03.017.

[35] Wells, G. N., and Dung, N. T., "A C0 discontinuous Galerkin formulation for Kirchhoff plates," *Computer Methods in Applied Mechanics and Engineering*, Vol. 196, No. 35-36, 2007, pp. 3370–3380. https://doi.org/10.1016/j.cma.2007.03.008.

[36] Noels, L., and Radovitzky, R., "A new discontinuous Galerkin method for Kirchhoff–Love shells," *Computer Methods in Applied Mechanics and Engineering*, Vol. 197, No. 33-40, 2008, pp. 2901–2929. https://doi.org/10.1016/j.cma.2008.01.018.

[37] Noels, L., "A discontinuous Galerkin formulation of non-linear Kirchhoff–Love shells," *International journal for numerical methods in engineering*, Vol. 78, No. 3, 2009, pp. 296–323. https://doi.org/10.1002/nme.2489.

[38] Bösing, P. R., Madureira, A. L., and Mozolevski, I., "A new interior penalty discontinuous Galerkin method for the Reissner–Mindlin model," *Mathematical Models and Methods in Applied Sciences*, Vol. 20, No. 08, 2010, pp. 1343–1361. https://doi.org/10.1142/S0218202510004623.

[39] Talamini, B. L., and Radovitzky, R., "A discontinuous Galerkin method for nonlinear shear-flexible shells," *Computer methods in applied mechanics and engineering*, Vol. 303, 2016, pp. 128–162. https://doi.org/10.1016/j.cma.2016.01.001.

[40] Gulizzi, V., Benedetti, I., and Milazzo, A., "An implicit mesh discontinuous Galerkin formulation for higher-order plate theories," *Mechanics of Advanced Materials and Structures*, Vol. 27, No. 17, 2020, pp. 1494–1508. https://doi.org/10.1080/15376494.2018.1516258.

[41] Guarino, G., Milazzo, A., and Gulizzi, V., "Equivalent-Single-Layer discontinuous Galerkin methods for static analysis of multilayered shells," *Applied Mathematical Modelling*, Vol. 98, 2021, pp. 701–721. https://doi.org/10.1016/j.apm.2021.05.024.

[42] Guarino, G., Gulizzi, V., and Milazzo, A., "High-fidelity analysis of multilayered shells with cut-outs via the discontinuous Galerkin method," *Composite Structures*, Vol. 276, 2021, p. 114499. https://doi.org/10.1016/j.compstruct.2021.114499.

[43] Gulizzi, V., Benedetti, I., and Milazzo, A., "A high-resolution layer-wise discontinuous Galerkin formulation for multilayered composite plates," *Composite Structures*, 2020, p. 112137. https://doi.org/10.1016/j.compstruct.2020.112137.

[44] Versino, D., Mourad, H. M., Williams, T. O., and Addessio, F. L., "A global–local discontinuous Galerkin finite element for finite-deformation analysis of multilayered shells," *Computer Methods in Applied Mechanics and Engineering*, Vol. 283, 2015, pp. 1401–1424. https://doi.org/10.1016/j.cma.2014.10.017.

[45] Benedetti, I., Gulizzi, V., and Milazzo, A., "Layer-Wise Discontinuous Galerkin Methods for Piezoelectric Laminates," *Modelling*, Vol. 1, No. 2, 2020, pp. 198–214. https://doi.org/10.3390/modelling1020012.

[46] Antonietti, P. F., Buffa, A., and Perugia, I., "Discontinuous Galerkin approximation of the Laplace eigenproblem," *Computer methods in applied mechanics and engineering*, Vol. 195, No. 25-28, 2006, pp. 3483–3503. https://doi.org/10.1016/j.cma.2005.06.023.

[47] Giani, S., and Hall, E. J., "An a posteriori error estimator for hp-adaptive discontinuous Galerkin methods for elliptic eigenvalue problems," *Mathematical Models and Methods in Applied Sciences*, Vol. 22, No. 10, 2012, p. 1250030. https://doi.org/10.1142/S0218202512500303.

[48] Buffa, A., and Perugia, I., "Discontinuous Galerkin approximation of the Maxwell eigenproblem," *SIAM Journal on Numerical Analysis*, Vol. 44, No. 5, 2006, pp. 2198–2226. https://doi.org/10.1137/050636887.

[49] Buffa, A., Houston, P., and Perugia, I., "Discontinuous Galerkin computation of the Maxwell eigenvalues on simplicial meshes," *Journal of computational and applied mathematics*, Vol. 204, No. 2, 2007, pp. 317–333. https://doi.org/10.1016/j.cam.2006.01.042.

[50] Hesthaven, J. S., and Warburton, T., "High–order nodal discontinuous Galerkin methods for the Maxwell eigenvalue problem," *Philosophical Transactions of the Royal Society of London. Series A: Mathematical, Physical and Engineering Sciences*, Vol. 362, No. 1816, 2004, pp. 493–524. https://doi.org/10.1098/rsta.2003.1332.

[51] Cliffe, K. A., Hall, E. J., and Houston, P., "Adaptive discontinuous Galerkin methods for eigenvalue problems arising in incompressible fluid flows," *SIAM Journal on Scientific Computing*, Vol. 31, No. 6, 2010, pp. 4607–4632. https://doi.org/10.1137/080731918.

[52] Meng, J., and Mei, L., "Discontinuous Galerkin methods of the non-selfadjoint Steklov eigenvalue problem in inverse scattering," *Applied Mathematics and Computation*, Vol. 381, 2020, p. 125307. https://doi.org/10.1016/j.amc.2020.125307.

[53] Saye, R. I., "High-Order Quadrature Methods for Implicitly Defined Surfaces and Volumes in Hyperrectangles," *SIAM Journal on Scientific Computing*, Vol. 37, No. 2, 2015, pp. A993–A1019. https://doi.org/10.1137/140966290.

[54] Ciarlet, P. G., "An introduction to differential geometry with applications to elasticity," *Journal of Elasticity*, Vol. 78, No. 1-3, 2005, pp. 1–215. https://doi.org/10.1007/s10659-005-4738-8.

[55] Carrera, E., "Theories and finite elements for multilayered, anisotropic, composite plates and shells," *Archives of Computational Methods in Engineering*, Vol. 9, No. 2, 2002, pp. 87–140. https://doi.org/10.1007/BF02736649.

[56] Sciascia, G., Oliveri, V., Milazzo, A., and Weaver, P. M., "Ritz Solution for Transient Analysis of Variable-Stiffness Shell Structures," *AIAA Journal*, Vol. 58, No. 4, 2020, pp. 1796–1810. https://doi.org/10.2514/1.J058686.

[57] Jones, R., *Mechanics Of Composite Materials*, Materials Science and Engineering Series, Taylor & Francis, 1998.

[58] Ting, T., *Anisotropic Elasticity: Theory and Applications*, Oxford Engineering Science Series, Oxford University Press, 1996. URL https://books.google.it/books?id=RxBoH9GyPkEC.

[59] Arnold, D. N., Brezzi, F., Cockburn, B., and Marini, L. D., "Unified analysis of discontinuous Galerkin methods for elliptic problems," *SIAM journal on numerical analysis*, Vol. 39, No. 5, 2002, pp. 1749–1779. https://doi.org/10.1137/S0036142901384162.

[60] Saye, R., "Implicit mesh discontinuous Galerkin methods and interfacial gauge methods for high-order accurate interface dynamics, with applications to surface tension dynamics, rigid body fluid–structure interaction, and free surface flow: Part I," *Journal of Computational Physics*, Vol. 344, 2017, pp. 647–682. https://doi.org/10.1016/j.jcp.2017.04.076.

[61] Saye, R. I., "Efficient multigrid solution of elliptic interface problems using viscosity-upwinded local discontinuous Galerkin methods," *Communications in Applied Mathematics and Computational Science*, Vol. 14, No. 2, 2019, pp. 247–283. https://doi.org/10.2140/camcos.2019.14.247.

[62] Saye, R., "Fast multigrid solution of high-order accurate multiphase Stokes problems," *Communications in Applied Mathematics and Computational Science*, Vol. 15, No. 2, 2020, pp. 147–196. https://doi.org/10.2140/camcos.2020.15.33.

[63] Gulizzi, V., Almgren, A. S., and Bell, J. B., "A coupled discontinuous Galerkin-Finite Volume framework for solving gas dynamics over embedded geometries," *Journal of Computational Physics*, 2022. https://doi.org/10.1016/j.jcp.2021.110861.

[64] Gulizzi, V., and Saye, R., "Modeling wave propagation in elastic solids via high-order accurate implicit-mesh discontinuous Galerkin methods," *Computer Methods in Applied Mechanics and Engineering*, Vol. 395, 2022, p. 114971. https://doi.org/10.1016/j.cma.2022.114971.

[65] Smith, M., *ABAQUS 6.14 Documentation*, Dassault Systèmes, 2014. Providence, RI, USA.

[66] Rogers, D. F., *An Introduction to NURBS: With Historical Perspective*, Morgan Kaufmann Publishers Inc., 2001.

[67] Piegl, L., and Tiller, W., *The NURBS Book (monographs in visual communication)*, Springer, 1997.